






Middle Triassic evaporite sedimentation in the Catalan basin: Implications for the paleogeographic evolution in the NE Iberian platform


F.  f.orti@ub.edu

J.M.  josepm.salvany@upc.edu


L.  lrosell@ub.edu

X.  [X. Castellort](#)^c

M.  m.ingles@ub.edu

E.  e.playa@ub.edu

^aDepartament de Mineralogia, Petrologia i Geologia Aplicada, Facultat de Ciències de la Terra, Universitat de Barcelona, C/ Martí i Franquès, s/n, 08028 Barcelona, Spain

^bDepartament  Enginyeria Civil i Ambiental, Universitat Politècnica de Catalunya, C/ Jordi Girona, 1-3, 08034 Barcelona, Spain




^cDepartament de Medi Ambient i Ciències del Sòl, Universitat de Lleida, C/ Av. Alcalde Rovira i Roure 191, 25198 Lleida, Spain

*Corresponding author.

Editor: Dr. B. Jones

Abstract

The eastern sector of the epicontinental Iberian platform underwent restriction after the sedimentation of the lower Muschelkalk carbonates (Middle Triassic) under extensional regime. This resulted in the accumulation of the marine evaporites and the alluvial siliciclastics of the middle Muschelkalk facies in the Triassic Catalan basin, which varied between 100 and 120 m in thickness. This facies consists of three lithostratigraphic units sedimented at basin scale (Lower, Middle and Upper), each of which includes a distinct evaporite unit. In the Lower Unit, the evaporitic sedimentation started as a transgressive sulfate lagoon (Paüls Gypsum unit). During the Middle Unit time, a regressive evaporitic mudflat, made up of a mosaic of shallow gypsum salinas surrounded by anhydrite sabkhas (Arbolí Gypsum unit) developed; in the northeastern half of the basin, an alluvial plain was formed by siliciclastics (Guanta Sandstone unit) of a west and northwest provenance (Lleida High). During the Upper Unit time, a new transgressive sulfate lagoon occupied the southern half of the basin (Camposines Gypsum), whereas an evaporitic mudflat of red-to-variegated mudstones, marls, and lacustrine carbonates developed in the northern half. Cyclic sedimentation was mainly recorded in the evaporitic mudflat-alluvial plain complex of the Middle Unit. The sulfur isotopic values of gypsum in the three evaporite units show a decrease in $\delta^{34}\text{S}$ with time and also a clear distinction from the values of the Keuper facies in the basin. A division of the lithostratigraphic succession into two third-order depositional sequences is proposed. The middle Muschelkalk succession in the Catalan basin is compared with the equivalent one in the subsurface of the adjacent Triassic Maestrat basin, which was filled with >600 m of marine evaporites.

Keywords:  Evaporites;  Sedimentation;  Sulfate isotopy; Muschelkalk; Triassic; Iberian platform

1.1 Introduction

During the Middle-Upper Triassic, a series of carbonatic and evaporitic episodes was recorded in the stratigraphical successions of the westernmost Neotethysian domain (Simms and Ruffel, 1989). The stratigraphic-sedimentologic research of these successions has been traditionally focused on the carbonate deposits in the areas of that ancient domain which today form part of western and central Europe. Less attention, however, has been dedicated to the study of the associated evaporites despite the fact that they would yield insight into the paleogeographic evolution of the domain.

The Iberian Plate (Iberia), which was part of this wide domain, recorded an exceptional sedimentation of evaporites in its epicontinental, eastern platform during the Middle Triassic to Early Jurassic time interval. Such a record consists of the following facies and units from base to top: Röt facies, middle Muschelkalk facies, lower Keuper unit, upper Keuper units, and Anhydrite Zone (Ortí et al., 2017). Of the evaporites of this record, the extensive Keuper evaporites (Carnian-Norian; Upper Triassic) are the best known. The Keuper evaporites had a clear precursor in the middle Muschelkalk evaporites of the Middle Triassic, which accumulated in the easternmost sector of the Iberian platform. The middle Muschelkalk evaporites, however, are little known because their outcrops are limited to the NE of the Iberian Peninsula and because they display similar characteristics to those of the Keuper. The Catalan Coastal Ranges, where many outcrops of these evaporites occur, were selected for the present study. These outcrops correspond to the ancient Triassic Catalan basin.

This paper seeks to improve the understanding of some fundamental aspects of the middle Muschelkalk evaporites in NE Iberia (stratigraphy, paleogeography, cyclicity, sulfate isotopy, relationships with the coeval detrital sediments, and third-order depositional sequences). The paper also provides tools for better discriminating the middle Muschelkalk evaporites from those of the Keuper. Hence, our study will complement the documentation on the middle Muschelkalk siliciclastic facies already available for this basin (Castelltort, 1986; Morad et al., 1995). This will also increase the understanding of the sedimentologic and paleogeographic evolution of the eastern Iberian platform during the Middle Triassic time.

2.2 Geological setting

The Triassic Catalan basin was a NE-SW elongated basin located in the northeastern sector of the epicontinental Iberian platform (Ortí et al., 2017) (Fig. 1A). Towards the W, this basin was separated from the Triassic Ebro basin by the Lleida High, which is currently buried beneath the Mesozoic and Paleogene deposits of the present Ebro Valley (Castillo Herrador, 1974). This paleohigh connected in a NE direction with the Montseny Massif that currently emerges up to 1700 m above the sea level. Both the Lleida High and the Montseny Massif are composed mainly of granitic and metamorphic Paleozoic rocks of the Variscan orogeny. Towards the SW, the Triassic Catalan basin was connected with the Triassic Maestrat basin, which at present remains buried under a thick cover of post-Triassic (mainly Cretaceous) rocks. Towards the east, beyond the present-day coastal line, the continuation of both the Catalan and the Maestrat basins underneath the ~~Mediterranean~~ Mediterranean Sea is poorly documented.

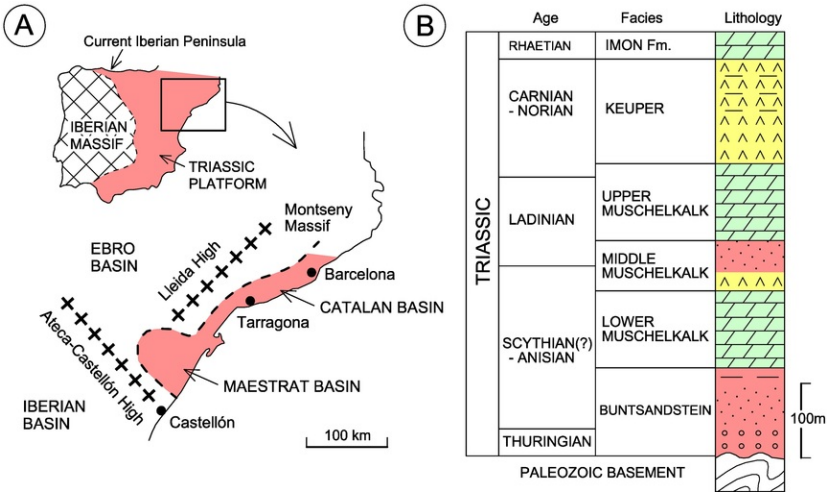


Fig. 1 (A) Location in the Iberian Peninsula of the Triassic Catalan and Maestrat basins, and other Triassic basins. The paleogeographical highs of Lleida and Ateca-Castellón (after Castillo Herrador, 1974) are indicated. (B) Stratigraphic succession in the Triassic Catalan basin (age of the facies taken from Calvet and Marzo, 1994, fig. 14).

alt-text: Fig. 1

The rocks of the Triassic Catalan basin crop out along the Catalan Coastal Ranges (CCR), which extend parallel to the Mediterranean coast (Fig. 2). In a SE to NW direction, the CCR are structurally formed by the Littoral and

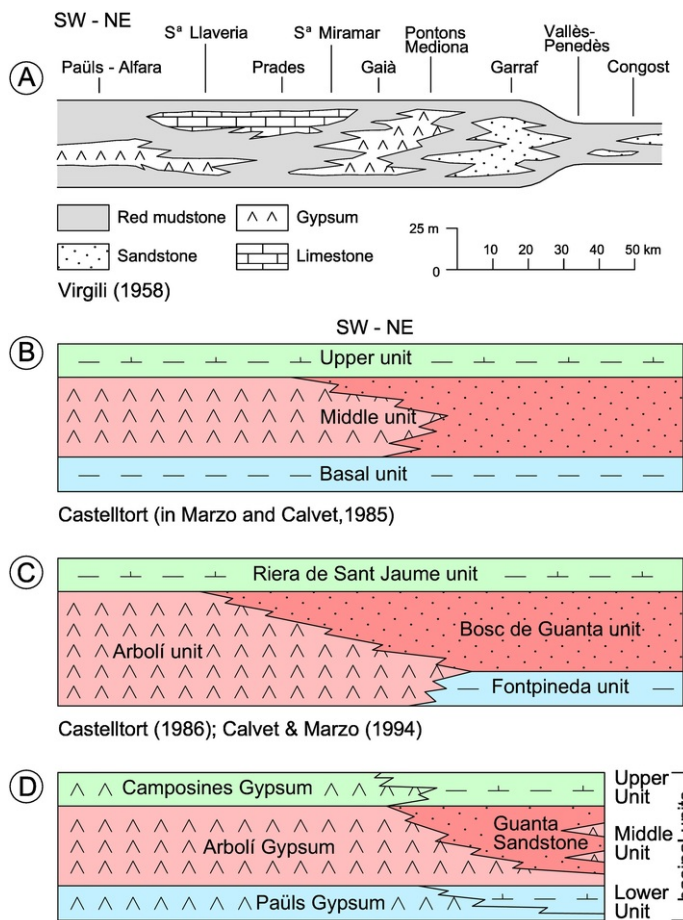


Fig. 3 Two-dimensional stratigraphic schemes, out of scale, of the middle Muschelkalk facies in the Catalan Coastal Ranges according to several authors. (A): Virgili (1958); (B): Castelltort (in Marzo and Calvet, 1985); (C): Castelltort (1986) and Calvet and Marzo (1994); (D): present work.

alt-text: Fig. 3

3.3 Methods

Lithofacies description was carried out in polished slabs of selected samples, and thin sections of 35 gypsum samples were prepared for petrographic study. Samples of gypsum and mudstones (siliciclastic deposits of <60 µm in grain size) were selected for mineralogical identification by X-ray diffraction (XRD) analysis. All the XRD analyses were performed in the CCiTUB (Universitat de Barcelona) using a PANalytical X^oPert PRO MPD Alpha1 powder diffractometer in Bragg-Brentano $\theta/2\theta$ geometry of 240 ~~millimeters~~mm of radius and Cu K α_1 radiation ($\lambda = 1.5406 \text{ \AA}$).

In the present article, 178 samples of mudstone beds were taken in eight of the stratigraphic sections studied (Fig-2Table 1). For the clay mineral analysis of these samples, a portion of each one was disaggregated and deflocculated by successive washing with distilled water. The <4 µm size fraction was separated by centrifugation. Oriented specimens were prepared for X-ray diffraction by smearing a paste of <4 µm fraction onto a glass slide to minimize size fractionation of the clay particles (Moore and Reynolds, 1989). Identification of clay mineral phases was made after air-drying, ethylene glycol solvation at 55 °C for 24 ~~hours~~h, and heating at 550 °C for 2 ~~hours~~h the oriented mounds.

Thirty eight gypsum samples, collected from all the sections under study, were selected for isotope analysis. In addition, the sulfate isotope composition of 156 gypsum samples of Keuper units of the Catalan basin was analysed for comparison. For the same purpose, four anhydrite core samples from a deep drill intersecting the middle Muschelkalk interval in the subsurface of the adjacent Maestrat basin were isotopically analysed.

For the isotopic analysis, each sample was dissolved in distilled water, acidified to pH 3 adding HCl and then reprecipitated as barium sulfate by means of a solution of BaCl₂. Sulfur and oxygen isotope compositions were analysed by the *on-line* method. The δ³⁴S_{V-CDT} was determined with a Carlo Erba 1108 Elemental ~~Analyzer~~ Analyser and the δ¹⁸O_{V-SMOW} with a TC-EA unit, both coupled to an IRMS ThermoFisher Delta Plus XP at the Stable Isotope Laboratory of the CCiTUB (Universitat de Barcelona). The obtained δ³⁴S and δ¹⁸O values are reported in ‰ relative to the Vienna Canyon Diablo Troilite (V-CDT) standard for sulfur and to the Vienna SMOW (V-SMOW) standard for oxygen. The analytical error (2σ) was ±0.4‰ for δ³⁴S and ±0.5‰ for δ¹⁸O. Isotope compositions obtained by the Standard IAEA NBS-127 were of 20.3‰ for δ³⁴S, and of 9.3‰ for δ¹⁸O. Isotope compositions obtained for δ³⁴S by the Standard IAEA SO-5 were of 0.5‰ and by the Standard IAEA SO-6 were of -34.1‰.

4.4 Mineralogy and evaporite petrology

Morad et al. (1995) studied the very fine fraction (<2 μm) of the siliciclastic matrix present in sandstone samples of the middle Muschelkalk facies coming from several of the stratigraphic sections initially studied by Castellort (1986) along the CCR. In this <2 μm fraction of the sandstones, the clay minerals were present as interstitial matrix mixed with dolomite, and as grain coatings. In the interstitial matrix, the clay minerals were mixed-layer illite/smectite, regularly (corrensite) and irregularly (70:30), interstratified chlorite/smectite, and minor kaolinite.

The mineralogy of the mudstone beds interbedded in the sandstone layers of the middle Muschelkalk facies of the Triassic Catalan basin was studied in Cabañeros and Masriera (1977). These authors found illite with good crystallinity as the major clay mineral, and also cited the possible presence of a poorly crystallized, interstratified or clay mineral of the chlorite or ‘montmorillonite’ types.

In the present work, the main clay minerals identified in the mudstone samples (Table 1) were illite and chlorite, and in some sections small amounts of expansive stratified minerals were found. Besides, variable amounts of quartz, dolomite, magnesite, gypsum, feldspars, and hematite were present. This clay mineral association mainly reflects clastic origin.

Table 1 Mineralogy (XR diffraction) of sulfate, carbonate, and mudstone samples of the middle Muschelkalk facies in the Triassic Catalan basin.				
alt-text: Table 1				
Locality	Unit	Sample	Lithology	Mineralogy ^a
Middle Muschelkalk samples				
Paüls quarry	Camposines	MPA-4	Secondary gypsum	gyp (88%), dol (5%), anh (3%), q (2%), cel (2%)
	Arbolí	MPA-3	Secondary gypsum	gyp (83%), q (12%), anh (3%), ru (2%)
	Paüls	MPA-1	Secondary gypsum	gyp (83%), anh (11%), dol (6%)
Venta De Camposines section	Camposines	MVC-6	Secondary gypsum	gyp (68%), mgs (11%), cal (7%), q (8%), cel (6%)
	Camposines	MVC-8	Secondary gypsum	gyp (95%), anh (5%)
	Camposines	MVC-9	Secondary gypsum	gyp (70%), q (13%), dol (12%), anh (3%), ru (2%)
	Paüls	MVC-2	Secondary gypsum	gyp (66%), dol (23%), anh (5%), cel (6%)
Masriudoms quarries	Paüls	MMR-1	Secondary gypsum	gyp (92%), mgs (4%), anh (4%)
	Paüls	MMR-2	Mudstone	I, Ch, Ex (traces)
	Paüls	MMR-3	Mudstone	I, Ch, Ex (traces)
	Paüls	MMR-5	Secondary gypsum	gyp (85%), q (10%), anh (3%), ru (2%)
Pratdip section	Camposines	MPT-1	Mudstone	I, Ch, Sm
	Arbolí	MPT-2	Secondary gypsum	gyp (88%), dol (10%), q (2%)
	Arbolí	MPT-3	Mudstone	I, Ch, Ex (traces)

	Arbolí	MPT-4	Mudstone	I, Ch
Pradell quarry	Paüls	MPR-2	Secondary gypsum	gyp (79%), dol (8%), cal (6%), cel (3%), q (2%), anh (2%)
	Paüls	MPR-3	Secondary gypsum	gyp (89%), dol (7%), cel (4%)
Coll de Falset section	Arbolí	MCF-2	Secondary gypsum	gyp (77%), dol (12%), q (7%), anh (4%)
	Paüls	MCF-1	Secondary gypsum	gyp (92%), dol (8%)
Arbolí section	Paüls	MAR-1 +	Secondary gypsum	gyp (95%), cal (3%), q (1%), cel (1%)
	Arbolí	MAR-3 +	Secondary gypsum	gyp (94%), dol (4%), cel (2%)
	Arbolí	MAR-4 +	Mudstone	I, Ch
	Arbolí	MAR-5 +	Mudstone	I, Ch
	Arbolí	MAR-7 +	Mudstone	I, Ch
	Arbolí	MAR-10 +	Secondary gypsum	gyp (70%), dol (28%), cel (2%), (hal)
	Arbolí	MAR-11bis +	Mudstone	I, Ch
Rojalons section	Arbolí	MRO-2	Secondary gypsum	gyp (96%), q (2%), cel (2%)
	Arbolí	MRO-3	Secondary gypsum	gyp (72%), q (15%), dol (9%), anh (3%), ru (1%)
	Camposines	MRO-6	Mudstone	I, Ch
Querol composite section	Arbolí	MQE-1	Mudstone	I, Ch
	Arbolí	MQE-2	Mudstone	I, Ch
	Camposines	MQE-3	Mudstone	I, Ch
	Camposines	MQE-5 inferior	Secondary gypsum	gyp (46%), dol (38%), q (12%), anh (2%), cel (1%), ru (1%) (mus)
	Camposines	MQE-7	Mudstone	I, Ch
	Paüls	MQE-8	Secondary gypsum	gyp (86%), dol (13%), q (1%)
	Arbolí	MQE-12	Mudstone	I, Ch
	Arbolí	MQE-13	Secondary gypsum	gyp (85%), dol (7%), q (7%), ru (1%)
Corbera section	Arbolí	MFP-5	Secondary gypsum	gyp (59%), dol (27%), q (9%), anh (4%), ru (1%) (I)
Vallirana mine	Paüls	MVA-1	Mudstone	I, Ch
	Paüls	MVA-3	Secondary gypsum	gyp (77%), anh (12%), dol (6%), q (2%), cel (2%)
	Paüls	MVA-5	Secondary gypsum	gyp (66%), anh (31%), dol (2%)
Figaró section	Arbolí	MFG-1	Mudstone	I, Ch
	Arbolí	MFG-2	Secondary gypsum	gyp (97%), q (3%)
	Arbolí	MFG-4	Secondary gypsum	gyp (85%), dol (7%), anh (5%), q (3%)
Aiguafreda section	Arbolí	MMC-1	Secondary gypsum	guix (99%), quars (1%)
	Arbolí	MMC-3	Secondary gypsum	gyp (64%), dol (28%), q (4%), anh (4%)
La Puda mine	Paüls	MLP-4	Secondary gypsum	gyp (88%), q (5%), an (2%), cal (2%), cel (2%), ru (1%)
	Arbolí	MLP-7	Secondary gypsum	gyp (91%), q (2%), dol (4%), cel (1%), cal (1%)

Bobalar-1 borehole (Maestrat Basin)	Undetermined	M2-(Tc10)	Anhydrite	anh (93%), mgs (5%), q (2%), (ru, mus)
	Undetermined	M5-(Tc10)	Anhydrite	anh (96%), q (2%), mgs (1%)
	Undetermined	M13-(Tc11)	Anhydrite	anh (96%), mgs (2%), hal (1%), q (<1%), ru (<1%)
	Undetermined	M14-(Tc11)	Anhydrite	anh (85%), mgs (8%), q (5%), ru (1%), zr (1%)
Keuper samples				
Rasquera	Miravet	RA12	Secondary gypsum	gyp (88%), q (4%), anh (4%), cel (2%), cal (2%)
Espinagosa	Miravet	ES5	Anhydrite	anh (99%), mgs (1%)
	Miravet	ES7	Secondary gypsum	gyp (85%), dol (9%), anh (2%), q (2%), cel (2%)
	Miravet	ES14	Anhydrite	anh (84%), dol (10%), gyp (6%)
	El Molar	ES22	Secondary gypsum	gyp (83%), q (8%), mgs (6%), anh (3%)
	El Molar	ES24	Secondary gypsum	gyp (72%), anh (9%), ar (8%), q (7%), cal (3%), cel (2%)
Gallicant	El Molar	GA28	Secondary gypsum	gyp (82%), anh (8%), mgs (5%), q (3%), cel (2%)
	El Molar	GA29	Secondary gypsum	gyp (88%), cel (6%), q (4%), anh (3%)
Corbera	Miravet	CO3	Secondary gypsum	gyp (82%), anh (8%), mgs (5%), q (3%), cel (2%)
	Miravet	CO16	Anhydrite	anh (97%), dol (1%), q (2%)
	El Molar	CO23	Secondary gypsum	gyp (50%), anh (43%), q (3%), mgs (3%), cel (1%)

Minerals: anh anhydrite; ar aragonite; cal calcite; cel celestite; dol dolomite; gyp gypsum; hal halite; hem hematite; mgs magnesite; mus muscovite; q quartz; ru rutile; zr zircon.

Clays: Ch chlorite; Ex expansive clays; I illite; K kaolinite; S smectite.

^a Semiquantitative for secondary gypsum and anhydrite; for mudstones, the results correspond to the <2 μm fraction.

The mineralogy of the gypsum samples is shown in Table 1. Gypsum is usually accompanied by carbonate minerals, of which dolomite is the most abundant, although also calcite and occasionally magnesite are found. Quartz, anhydrite and celestite are common minerals, and less frequent minerals in some samples are muscovite, halite, rutile and zircon.

Common lithofacies of the gypsum rocks are laminated and nodular, and less frequently massive. However, all the gypsum rocks on outcrop, at quarry fronts or in mine galleries were identified as secondary gypsum, i.e. gypsum rocks which derived from the hydration of anhydrite rock close to the surface. Petrographically, this secondary gypsum was easily distinguished by means of their diagnostic alabastrine and porphyroblastic textures, and by the frequent presence of anhydrite relics in these textures. On outcrop, the secondary gypsum was identified by the presence of porphyroblasts, i.e. individual gypsum crystals, up to 1 cm in size, ovoid in shape and dark to greenish in color.

Apart from the sporadic observation of residual masses of anhydrite in some fronts of gypsum quarries, the presence of this mineral in the CCR is generalised at depths greater than those of common mine galleries, as formerly documented by Ortí and Bayó (1977) in samples coming from exploratory boreholes. In turn, much of this subsurface anhydrite was derived from the gypsum-to-anhydrite conversion of the original gypsum deposits during deep burial. Some of the anhydrite, however, could originate from synsedimentary growth in sabkha environments. This is mainly the case of the nodular lithofacies of the today’s secondary gypsum observed on outcrop.

Salt bodies have not been documented in the CCR. Only isolated pseudomorphs of halite crystals were observed by us very locally.


5.5 Evaporite units

Regional exploration in many Triassic outcrops, where the middle Muschelkalk facies is exposed, was carried out along the CCR from the Ebro River in the SW to the Montseny Massif in the NE. A number of stratigraphic sections of this facies were studied (Fig. 2), and their UTM coordinates are shown in Table 2. Depending on the local outcrop conditions, the sections are complete or partial. Some complete sections are predominantly evaporitic (Alfara, Paùls, Camposines, Vilella Baixa, Coll de Falset, Arbolí, Rojalons), others are mainly siliciclastic (Pontons, Esparreguera, Guanta), and others are mixed, siliciclastic-evaporitic (Querol, Corbera, Bigues, Figaró). Detailed studies

of these successions are complex due to (a) low exposure quality in many of the outcrops, (b) moderate to strong tectonic deformation favored by the plasticity of the clayey and evaporitic materials, (c) and possible evaporite dissolution close to the surface. All this often makes it difficult to correctly characterize the original succession, as well as the calculation (often only the estimation) of the depositional thicknesses. Moreover, the frequent interfingering both laterally and vertically between evaporites and siliciclastics masks the precise boundaries between the lithostratigraphic units.

Table 2 Coordinates UTM (UTM 31N/ETR-S89) of the sections.

alt-text: Table 2

Sections		Coordinates UTM		
		X	Y	Z
Alfara		280,154	4,527,586	350
Paùls		283,476	4,535,250	379
Camposines	Paùls Gypsum unit	295,750	4,552,508	253
Camposines	Arbolí Gypsum unit	295,049	4,552,524	191
Camposines	Camposines Gypsum unit	295,169	4,552,811	255
Vilella Baixa		310,110	4,566,946	260
Masriudoms		322,316	4,543,044	200
Pratdip		321,667	4,547,201	280
Coldejou		322,881	4,551,252	370
Pradell		321,594	4,557,551	455
Coll de Falset		319,437	4,557,303	537
Arbolí		328,600	4,566,524	785
Rojalons		345,655	4,578,898	841
Querol	Paùls Gypsum unit	365,748	4,585,810	531
Querol	Camposines Gypsum unit	365,656	4,587,286	435
Pontons		376,896	4,585,803	554
Corbera		412,211	4,585,908	265
Vallirana		411,045	4,579,891	226
Esparreguera		403,750	4,601,834	360
La Puda		406,304	4,602,901	154
Quanta		426,182	4,610,242	420
Bigues		434,002	4,615,899	317
Figaró		437,335	4,618,216	518
Aiguafreda		437,479	4,621,947	451

Schemes of all of the stratigraphic sections studied are shown in Fig. 4, and detailed representations, either total or partial, of some selected sections are displayed in Fig. 5. The profile of lateral correlation between these sections (Fig. 4) prompted us to use the three lithostratigraphic units formerly proposed by Castelltort (in Marzo and Calvet, 1985) at basin scale, i.e. basal, middle and upper, although under the new terms of Lower Unit, Middle Unit

and Upper Unit, respectively (Fig. 3D). The correlation profile (Fig. 4) also prompted us to distinguish the following evaporite units in association with each of the basinal units: Paùls Gypsum (in the Lower Unit), Arbolí Gypsum (in the Middle Unit), and Camposines Gypsum (in the Upper Unit). The isotopic values (see below, Section 6) of gypsum in the three evaporite units indicate the marine origin of the mother brines. A possible correlation of our basinal units with the lithologic groups of Virgili (1955, 1958) is shown in Table 3. This table also includes observations of other authors on the middle Muschelkalk facies in the CCR.

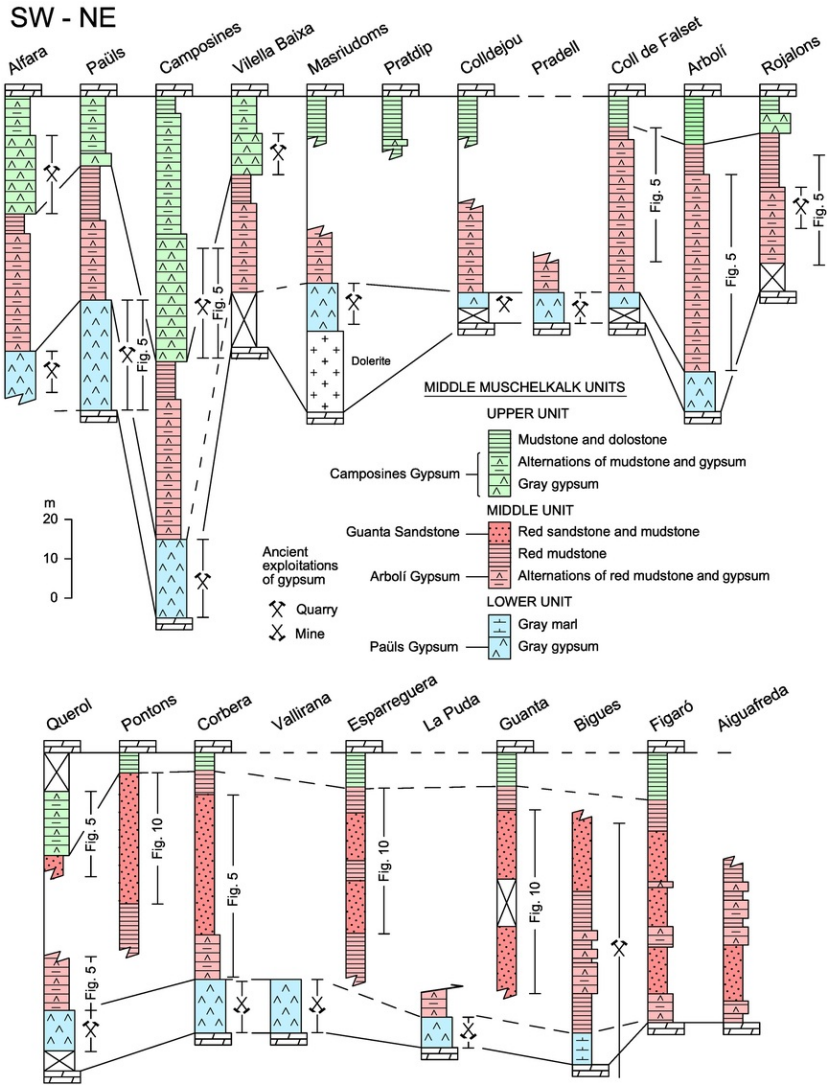


Fig. 4 Correlation profile of stratigraphic (simplified) sections in the middle Muschelkalk facies of the Catalan Coastal Ranges. The sections are arranged from the SW (Alfara section, upper part of the figure) to the NE (Aiguafreda section, lower part). Location of the sections in Fig. 2.

alt-text: Fig. 4

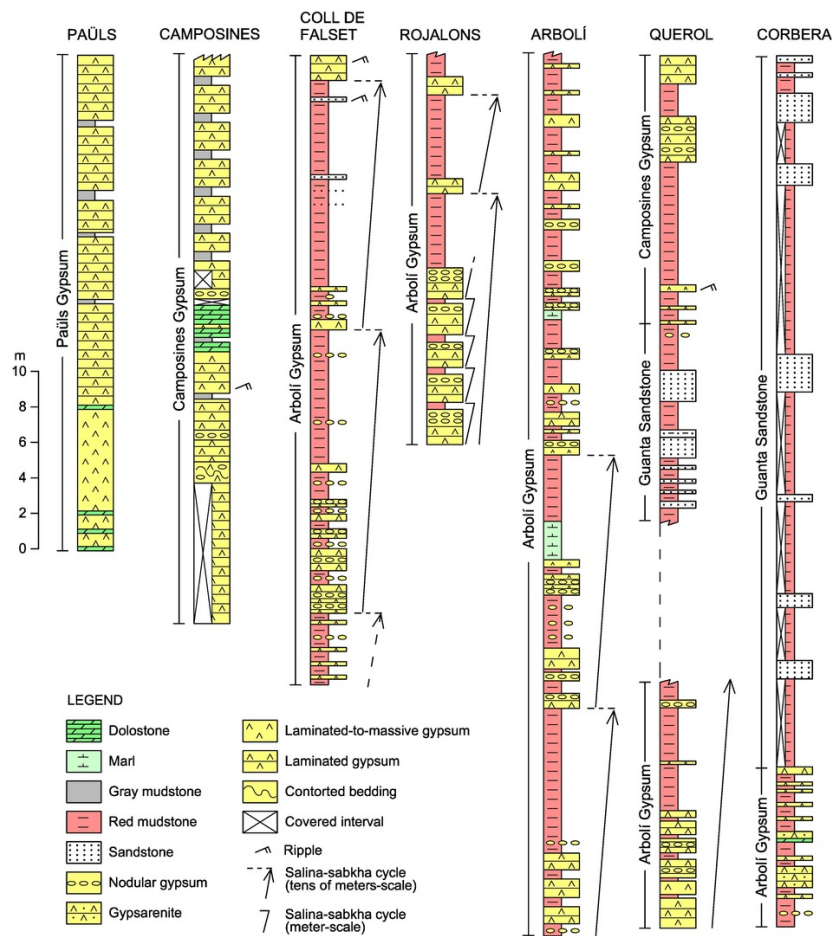


Fig. 5 Detailed intervals in some selected stratigraphic sections of the middle Muschelkalk facies in the Catalan Coastal Ranges. Some representative meter-scale cycles are shown in the Rojalons section. See Fig. 4 for the location of the intervals.

alt-text: Fig. 5

Table 3 Stratigraphic descriptions, according to different authors, of the middle Muschelkalk facies in the Triassic Catalan basin. CCR: Catalan Coastal Ranges.

alt-text: Table 3

Virgili (1955, 1958) (geographic sectors in the CCR according to Virgili, 1958)
“Stratigraphic conclusions” in the southern sector of the CCR (sections: Alfara, Paüls, Rasquera and Camposines) (p. 90–92): Intervals of the general succession in this sector:
- Yellowish and iridescent marls: 2–5 m (Top);
- Yellow or slightly red clays: 5–50 m of anhydrite and white or reddish gypsum with clay intercalations of the same tone: 18–60 m;
- Red clays that can contain fine gypsum veins: 10–15 m (Base).
“Stratigraphic conclusions” in the central sector of the CCR (sections: La Figuera-les Villes, Masroig-Guiamets, Llabería Ridge, Falset-Pradell, Prades Plateau, Miramar Ridge, Gaià Massif) (p. 251–252): Intervals of the general succession in this sector:
- Gray and blue marls with gypsum films in the central part: 5–15 m (Top);

- Red and iridescent clays that in the Gaia block (NW end of the central region) intercalate reddish, clayey sandstones: 35–60 m;
- Gypsum and anhydrite in thick layers intercalating thin beds of red and blue clays: 10–30 m
- Red and iridescent clays that locally (southern end of the sector) intercalate thin beds of red sandstones: 10–15 m (Base).
<i>“Stratigraphic conclusions” in the northern sector of the CCR (sections: Pontons-Mediona, margin of the Vallés-Penedés, Congost Valley, Badalona-Montgat, Garraf Massif) (p. 376–377): Intervals of the general succession in this sector:</i>
- Red and iridescent clay which in the uppermost beds is marly and yellowish: 4–15 m (Top);
- Clay-rich, red sandstone, which smoothly changes to the upper and lower levels: 10–30 m;
- Red and iridescent clay bearing gypsum and anhydrite intercalations; these intercalations may be absent or may reach up to 7 m in thickness: 15–30 m (Base).
Possible correlation between the stratigraphic intervals in Virgili (1955, 1958) and the units distinguished in this paper:
- The assemblage of the ‘yellowish, gray, iridescent and red marls’ horizon at the Top of the sections seems to be correlatable with the Upper Unit. However, the presence of important gypsum beds in this horizon (Camposines Gypsum unit in this paper) was not identified in Virgili (1955, 1958). Despite this, that author assumed local thicknesses up to 60 m for this assemblage (Alfara Valley, Virgili, 1958, p. 34, ‘yellowish marls with porous massive dolostones (‘carniolas’) levels’),
- The assemblage of gypsum and anhydrite intercalations within red or iridescent clays in the middle of the successions, up to 30 m in thickness, would correspond to the Arbolí Gypsum unit in this paper;
- The assemblage of red claystone horizon (Base) is not identified in this paper as an independent unit. Probably, this horizon was distinguished by Virgili (1958) in areas where the base of the Arbolí Gypsum unit is relatively poor in sulfates.
Calvet and Marzo (1994)
<i>The thickness of the whole succession varies from 50 to 115 m and can be divided into four units. From base to top and in E-W direction, the units are the following:</i>
- Fontpineda Lutite and Gypsum unit: it is formed by calcium sulfates deposited on a lutitic-evaporitic supratidal plain. It is 10–25 m thick;
- Bosc de Guanta Sandstone and Lutite unit: it occurs in the northern sector of the basin, while southwards it grades laterally into de Arbolí Gypsum unit. The materials of the Guanta Sandstone unit are interpreted as deposited by ephemeral flows in a terminal alluvial fan system;
- Arbolí Lutite and Gypsum unit: it is developed mainly in the southern sector of the basin. The setting of this unit corresponds to a playa-lake or to an evaporitic sabkha. It may reach almost one hundred 100 meters in thickness;
- Riera de Sant Jaume Lutite unit: it consists of gray-green lutites bearing millimetric-to-centimetric levels of carbonate. This unit is interpreted as deposited on a supralitoral supralittoral lutitic plain, and is overlain by the carbonates of the upper Muschelkalk facies throughout the basin. It is 5–10 m thick.
Ortí et al. (2017)
- In the Catalan basin, the middle Muschelkalk evaporites are associated with abundant siliciclastic host material (claystones in reddish or gray tones and sandstones);
- In the outcrops of the Catalan basin, sediments of clay-gypsum alternation salinas are observed in the lower gray unit of the successions, while sediments of clayey gypsum salinas and clayey sabkhas are present in the upper red unit. Sulfate lagoons are identified at the base of the succession in this basin (Ortí et al., 2017, fig. 8, M2 episode).

5.1.5.1 Paüls Gypsum unit

Esteban et al. (1977) reported that a carbonate crust forms the top of the lower Muschelkalk facies in the northern part of the Triassic Catalan basin (Fig. 6A, B), and Castellort (1986, fig. 9) distinguished a thick gypsum unit at the base of the middle Muschelkalk succession in some sections of the southern and central parts of the basin. These two observations were instrumental in defining our stratigraphy of the middle Muschelkalk succession. In fact, the Paüls Gypsum unit occurs in sharp contact with the underlying carbonate crust first reported by Esteban et al. (1977). This basal evaporite unit is very rich in sulfate, with only minor amounts of carbonate, marl, and clay allowing intensive exploitation throughout the basin. Gypsum beds display laminated (Fig. 6D) and massive (Fig. 6E) lithofacies, which are clear in tone, but also gray or dark locally. Nodular lithofacies and enterolithic levels were not observed in the gypsum beds.

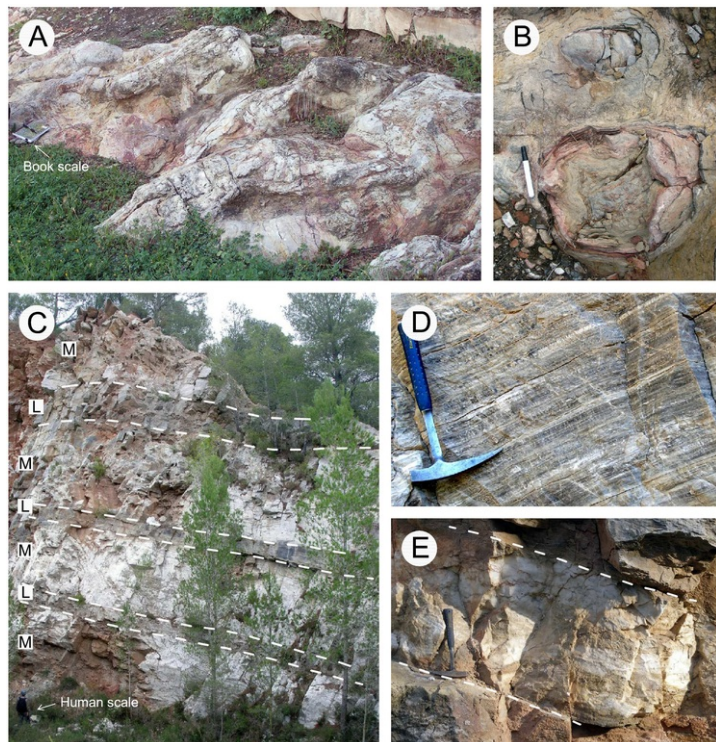


Fig. 6 Paüls Gypsum unit. (A) Dolomitic crust at the top of the lower Muschelkalk facies showing complex morphology (see book for scale). Corbera section. (B) Detail of the dolomitic crust in A: eroded domes showing internal lamination. (C) Lower part of the Paüls Gypsum unit in the quarry near the Paüls village (see human scale). Some meter-scale cycles can be observed which are formed by a thinner, gray laminated gypsum bed (L) at the base, and a thicker, white laminated to massive gypsum bed (M) at the top. (D) Detail of the gray, laminated gypsum lithofacies (small quarry in the Camposines section). (E) Detail of the white, massive gypsum lithofacies at the top of the meter-scale cycles (Pradell quarry). Hammer for scale.

alt-text: Fig. 6

This unit varies in thickness. In the southernmost part of the basin its thickness attains up to 30 m (Paüls, Alfara, and Camposines sections), although values between 5 and 20 m are common (Coll de Falset, Masriudoms, Coldejou, and Arbolí sections). The values in the central part are between 5 and 10 m (Querol section), and up to 15 m (Corbera and Vallirana mines, where thin laminae of dark claystones are interbedded with the laminated gypsum), although locally the thickness values are <5 m. In the northern part of the basin, the unit changes to some meters of dark mudstones, and it is followed upwards by few meters of marls and thin dolostone beds (Bigues section, Fig. 4). It should be noted, however, that the observation of this unit in some outcrops along the CCR is difficult because many of the ancient gypsum quarries are presently covered. Moreover, we were not able to identify the unit in some sections, because of structural disruption or local dissolution.

Depositional cycles are not very well developed in the Paüls Gypsum unit. A few cycles, generally of <1 m in thickness, can be found just at the base of the unit very locally (Paüls section, Fig. 5). They are formed by a thin lower carbonate bed and a thicker upper gypsum bed. Some metre-scale cycles, however, are found in the lower part of the unit in the Paüls and Pradell sections (Fig. 6C). The base of these cycles is made up of thinner beds of gray laminated gypsum and dark claystone, and the top is composed of thicker beds of laminated gypsum. Locally, however, massive gypsum overlies the laminated beds at the top of the cycle (Fig. 6E).

Two occurrences of thick gypsum deposits of unclear attribution are worthy of note. One is the gypsum unit in an old mine near La Puda site (Esparreguera) (Fig. 2), where the tectonic structure is complex. This unit was attributed to the top of the Buntsandstein siliciclastics (Röt facies) by Virgili (1958). However, we assign it to the Paüls Gypsum unit given that (1) we were not able to observe gypsum levels in the Röt facies in the surrounding areas, and (2) that the isotopic values of the gypsum in this mine are exactly the same as for the other gypsum samples of the middle Muschelkalk under study (see below). The other occurrence is the outcrop in the Montgat area near Barcelona, which was assigned to the middle Muschelkalk facies also by Virgili (1958). In this case, our isotopic values of gypsum clearly indicate a Keuper attribution (see below).

~~5.1.1.~~**5.1.1** *Interpretation*

Characteristics such as gypsum purity, predominance of laminated lithofacies, absence of nodular and enterolithic lithofacies, great depositional thickness, absence of exposure indicators (mudcracks, desiccation breccias, paleosoils) and distribution throughout the southern and central parts of the basin suggest that the unit was formed in a widespread sulfate lagoon with permanent gypsum precipitation. The maximum depth of this marine lagoon remains unknown, although it could be estimated at the meter-order. Presumably, it was located close to the open sea with a continuous supply of marine water. The presence at the base of some stratigraphic sections of meter-scale cycles displaying top levels of massive gypsum ([Fig. 6E](#)) has a doubtful interpretation, although this lithofacies does not show characteristics of sabkha deposits.

~~5.2.~~**5.2** **Arbolí Gypsum unit**

The Paüls Gypsum unit is overlain by the Arbolí Gypsum unit by means of gradual or rapid transition, depending on the stratigraphic sections. The Arbolí Gypsum unit is formed by an apparently irregular alternation of red mudstone beds and gypsum beds, with a total thickness ranging between 30 and 70 m. This red mudstone-gypsum alternation is the thickest and most characteristic evaporite facies association in the middle Muschelkalk succession in the basin ([Fig. 7A](#)). The gypsum beds, ranging between very few centimeters and >1 m in thickness, display laminated and nodular lithofacies and have variable tones. Tepee structures and microbial lamination ([Fig. 7D](#)) as well as some slumps at small scale are present in the laminated lithofacies. Nodular gypsum beds also occur, with variable amounts of reddish mudstone matrix. Gypsum nodules in these beds are white and display flattened and complex morphologies ([Fig. 7B](#)). The presence in this alternation of clastic gypsum levels (originally medium-grained gypsarenites) was observed locally (Corbera section) ([Fig. 7E](#)). As regards the mudstone beds, they have thicknesses ranging between very few centimeters and several meters. Although the mudstones are mostly red, some gray tones are found locally. Also marly mudstones are present in the alternation locally. Abundant satin-spar veins of gypsum that cements fractures can be present in the mudstone beds.

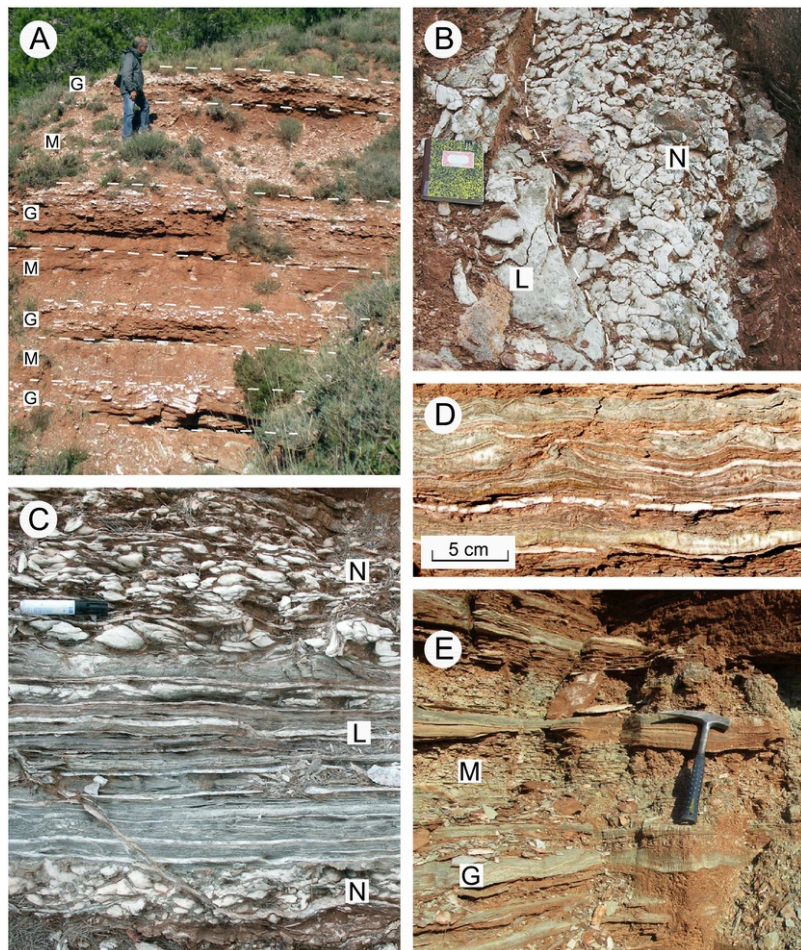


Fig. 7 Arbolí Gypsum unit. (A) Detail of the meter-scale, red mudstone (M)-gypsum (G) alternation in the Arbolí section, near the Arbolí village. Gypsum beds in this photograph display nodular lithofacies. (B) Top view of an alternation formed by nodular gypsum (N) at the base and laminated gypsum (L) at the top. Note the flattened morphology of the nodules. Book for scale. Camposines section. (C) Frontal view of an alternation of nodular gypsum (N) and laminated gypsum (L). Pen for scale. Coll de Falset section. (D) Microbial lamination in the gypsum beds. (E) Alternation of red mudstone (M) and laminated gypsum in the Corbera section. Some gypsum beds (G) were gypsarenites originally. [\(For interpretation of the references to color in this figure legend, the reader is referred to the web version of this article.\)](#)

alt-text: Fig. 7

Meter-scale depositional cycles are generalised in the red mudstone-gypsum alternation. A first type of cycle, which is very common, is formed by laminated gypsum at the base, nodular gypsum in the middle, and red mudstone at the top (Fig. 5, Rojalons section). A second type has also a thin level of nodular gypsum below the laminated gypsum. A third type lacks the top mudstone bed and only a gypsum alternation made up of laminated and nodular beds is observed (Fig. 7C). A fourth type of cycle is characterized by nodular gypsum beds that alternate with the red mudstone beds (Fig. 7A). The individual thickness of all of these cycles varies between <1 m and very few meters. The correlation of individual cycles in the various stratigraphic sections is difficult because of the structural complexity observed in many of the outcrops. The arrangement of these meter-scale cycles in some of the stratigraphic sections studied also suggest the presence of decameter-scale cycles (Fig. 5).

The Arbolí Gypsum unit extends throughout the Catalan Coastal Ranges. In the central and northern parts, however, this unit grades laterally into the Guanta Sandstone unit, which is characterized by an irregular alternation of red mudstone beds and sandstone beds (see below). Frequently, however, the gradation is not complete and some gypsum beds remain below the siliciclastic alternation (Fig. 4). Nevertheless, the tops of the two units composing the Middle Unit (Arbolí Gypsum and Guanta Sandstone) show predominance of red mudstones throughout the basin.

5.2.1.5.2.1 Interpretation (Arbolí Gypsum unit)

Overlying the sulfates of the Paüls Gypsum unit, the development of the widespread alternations formed by red mudstone beds and gypsum beds indicates shallower water conditions in the restricted basin. Numerous sulfate salinas, in which laminated gypsum precipitated, occupied a red mudflat. The salinas graded laterally into peripheral sabkhas, in which nodular anhydrite grew interstitially within reddish mudstone acting as matrix. The first type of meter-scale cycle mentioned above is an inundation cycle in which a gypsum salina develops rapidly on the red mudflat; subsequently the salina dries off and anhydrite nodules grow interstitially within the red mudstone; finally, only red mudstones become ~~predominat~~predominant. In the second type of cycle, the inundation occurs slowly and a sabkha stage develops before the development of the salina. In the third type of cycle, salina and sabkha stages alternate in the almost total absence of red mudstones. The fourth type of cycle corresponds to a sabkha setting in which the laminated gypsum lithofacies does not form. All these meter-scale cycles seem to be fifth-order cycles of a possible climatic (astronomic) origin. The decameter-order cycles (larger cycles of salina-sabkha; Fig. 5) seem to be fourth-order cycles, although the genetic control -climatic or tectonic- is uncertain. The paleogeographic scenario for the Arbolí Gypsum unit is an extensive, evaporitic, red mudflat lodging a mosaic of shallow salinas and sabkhas fed by marine water. This evaporitic mudflat was sensitive to record depositional cyclicity of high-frequency.

5.3.5.3 Camposines Gypsum unit

This evaporite unit is restricted to the southern part of the basin and locally to the central part. Maximum thickness, between 40 and 60 m, is recorded in the Alfara and Camposines sections (Fig. 4), and this value is similar to the one (60 m) assumed by Virgili (1958) for the ‘top yellowish marls’ in the Alfara valley (Table 1). In the Camposines and Alfara sections (Fig. 4), this unit shows a lower half which is very rich in gypsum beds with only minor carbonate laminae and thin claystone beds, which allowed small gypsum quarries in the past (Fig. 4 upper part). Gypsum lithofacies in this lower half is mainly laminated, (Fig. 8A, B). However, some beds of nodular gypsum, and rarely enterolithic gypsum are found also (Camposines section, Fig. 5). In the upper half of the section, gypsum beds alternate with variegated mudstones and marls. This alternation grades upwards into the upper Muschelkalk carbonates.

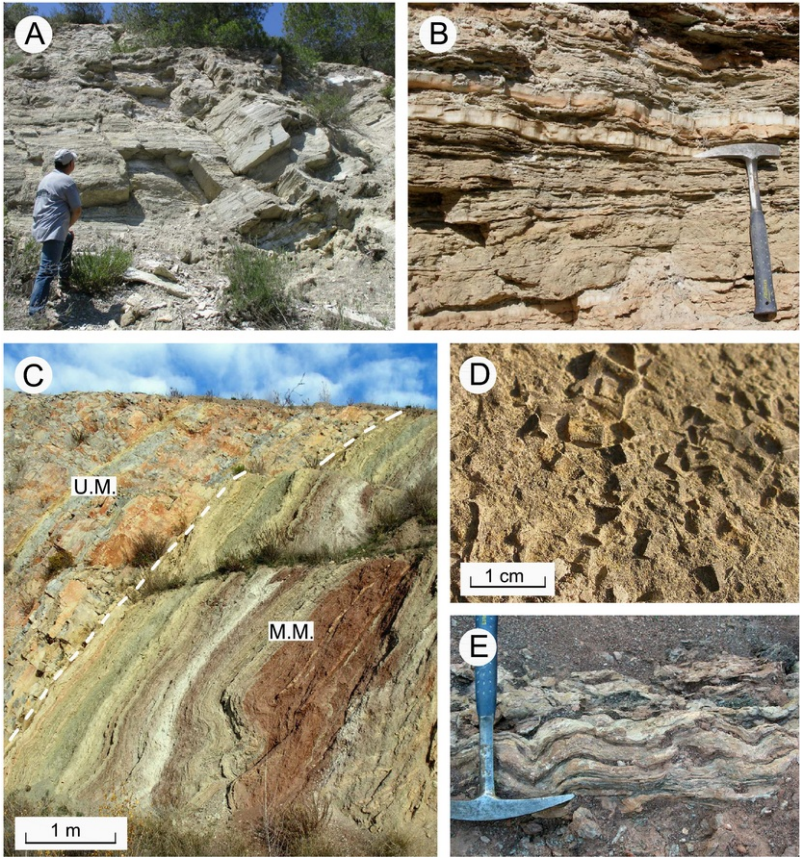


Fig. 8 Camposines Gypsum unit. (A) Small, ancient quarry front in the lower part of the Camposines Gypsum unit. Camposines section. The laminated gypsum lithofacies is predominant. (B) Laminated gypsum lithofacies. Some thick satin-spar gypsum veins are intercalated (pick of the hammer). Querol section. (C) Top of the Upper Unit (M.M.) of the middle Muschelkalk facies, dipping almost vertically, showing variegated mudstones, marls, and thin carbonate laminae (Guanta area). On the left of the photograph, the contact with the base of the upper Muschelkalk (U.M.) dolostones is observed. (D) Cast of cubic and hopper crystals of halite in a thin carbonate bed of the Upper Unit in the Pratsdip section. (E) Detail of C showing an alternation of undulated carbonate (microbial?) beds and much thinner laminae of red/gray mudstones. [\[For interpretation of the references to color in this figure legend, the reader is referred to the web version of this article.\]](#)

alt-text: Fig. 8

Thicknesses between 10 and 15 m for this unit were recorded in other sections of the southern and the central parts of the basin. In the Paüls section, the unit is formed by an irregular assemblage of gypsum beds and gray to reddish mudstone beds. In the Rojalons section, it is represented by some gypsum beds interlayered within variegated to gray mudstones. In the Pratsdip section, a single bed of laminated gypsum was found in association with red and ochre mudstone beds, and also with carbonate beds bearing casts of halite crystals (Fig. 8D). In the Querol section, several gypsum beds are present with a total thickness of 5 m in association with red to variegated mudstones. In a northeastern direction (Fig. 8C), this unit grades into mudstones, marls, and carbonate beds (Fig. 8E) with a total thickness of only 5 to 15 m, where evaporites were not observed.

5.3.1.5.3.1 Interpretation

Overlying the red mudflat at the top of the Arbolí Gypsum unit, the Camposines Gypsum unit indicates another marine flooding. The evaporites, however, were irregularly distributed in the basin and show the following lateral gradation of facies and environments. In a southern part of the basin (Alfara, Paüls, Camposines and Vilella Baixa sections; Fig. 4), where the evaporites are very thick and relatively pure, a marine sulfate lagoon developed. In the central part, the characteristics of the evaporites in the Querol (Fig. 5) and Rojalons (Fig. 4) sections only reflect the presence of salinas. In the northern part, where evidence of evaporite precipitation is absent, a marly mudflat with carbonate ponds was predominant (resembling the variegated Röt facies at the top of the Buntsandstein facies; Fig. 8C). This gradation also suggests the existence of a large sulfate lagoon towards the SW in the direction of the Triassic Maestrat basin. The evaporites of the southern part of the Catalan basin presumably represent the northeastern margin of this lagoon. In fact, the intercalation within the thick Camposines section of some nodular and enterolithic beds, which indicate some exposure episodes (Fig. 5), does not suggest a lagoonal depocenter.

6.6 Isotopes. Results and interpretation

The isotope compositions obtained in the present work for the marine evaporitic sulfates of the middle Muschelkalk facies of the Catalan basin (38 samples of secondary gypsum) range from 16.5 to 18.7‰ for δ³⁴S, and from 7.63 to 16.5‰ for δ¹⁸O (Table 4 and Fig. 9 upper part). The mean δ³⁴S values for the different evaporite units are the following: 18.3‰ (standard deviation: 0.28; *n*_i = 14) for the Paüls Gypsum unit; 17.7‰ (standard deviation: 0.48; *n*_i = 20) for the Arbolí Gypsum unit; and 16.6‰ (standard deviation: 0.10; *n*_i = 4) for the Camposines Gypsum unit (Fig. 9 lower part). The mean δ¹⁸O values for the different evaporite units are the following: 12.3‰ (standard deviation: 1.34; *n*_i = 14) for the Paüls Gypsum unit; 12.9‰ (standard deviation: 1.89; *n*_i = 20) for the Arbolí Gypsum unit; and 13.2‰ (standard deviation: 0.89; *n*_i = 4) for the Camposines Gypsum unit (Fig. 9 lower part). Additionally, four anhydrite samples taken in the middle Muschelkalk interval of the Bobalar-1 deep borehole in the neighbouring Triassic Maestrat basin (Bartrina and Hernández, 1990) were analysed for comparative purposes. The obtained values (Table 4) range from 17.3 to 17.5‰ in δ³⁴S and from 12.1 to 13.0 in δ¹⁸O.

Table 4 Isotope composition of sulfur (δ³⁴S_{V-CDT}) and oxygen (δ¹⁸O_{V-SMOW}) of the sulfate in gypsum samples of the middle Muschelkalk facies in the Triassic Catalan basin and, additionally, in four anhydrite samples from the deep borehole Bobalar-1 in the Maestrat basin. For comparison, some sulfate samples (gypsum and anhydrite) of the Keuper facies in the Triassic Catalan basin are included (stratigraphic sections from Salvany, 1986). Depths of the anhydrite samples in the Bobalar-1 borehole: M2 (core 10), 1782.3 m; M5 (core 10), 1787.3 m; M13 (core 11), 1857.0 m; M14 (core 11), 1858.0 m.

alt-text: Table 4

Locality	Sample	Unit	δ ³⁴ S _{V-CDT} ‰	δ ¹⁸ O _{V-SMOW} ‰
Middle Muschelkalk samples				
Paüls quarry	MPA-4	Arbolí	17.4	10.3
	MPA-3	Arbolí	18.4	15.0
	MPA-1	Paüls	18.2	11.5
	PAÜLS-1	Paüls	18	12.218
	PAÜLS-2	Paüls	18.4	12.12
	PAÜLS-3	Paüls	18.4	12.32

Venta De Camposines section	MVC-6	Camposines	16.7	13.5
	MVC-8	Camposines	16.5	12.7
	MVC-9	Camposines	16.6	14.3
	VC-1	Arbolí	17.5	12.44
	VC-2	Arbolí	17.1	12.31
	MVC-2	Paüls	18.1	15.5
Masriudoms quarries	MMR-1	Paüls	18.7	11.61
	MMR-5	Arbolí	17.5	16.5
Pratdip section	MPT-2	Arbolí	18.5	13.1
Pradell quarry	MPR-2	Paüls	18.2	14.3
	MPR-3	Paüls	18.7	13.3
Coll de Falset section	MCF-2	Arbolí	18.0	12.9
	MCF-1	Paüls	17.8	11.9
Arbolí section	MAR-3:	Arbolí	17.5	13.0
	MAR-10:	Arbolí	18.4	15.2
	MAR-1:	Paüls	18.5	11.80
Rojalons section	MRO-2	Arbolí	18.7	13.71
	MRO-3	Arbolí	17.2	12.67
Querol composite section	MQE-5 inferior	Camposines	16.5	12.3
	MQE-13	Arbolí	18.0	14.6
	MQE-8	Paüls	18.7	12.2
Corbera section	MFP-5	Arbolí	17.7	12.549
Vallirana mine	MVA-3	Paüls	18.3	12.436
	MVA-5	Paüls	18.1	11.89
La Puda mine	MLP-7	Arbolí	17.1	7.63
	MLP-4	Paüls	18.4	9.877
Figaró section	MFG-2	Arbolí	17.6	11.659
	MFG-4	Arbolí	17.5	11.877
	F-1	Arbolí	17.8	14.33
	F-2	Arbolí	17.9	13.879
Aiguafreda section	MMC-1	Arbolí	17.2	12.7
	MMC-3	Arbolí	17.6	12.2
Bobalar-1 borehole (Maestrat Basin)	M2-(Tc10)	Undetermined	17.5	13.0
	M5-(Tc10)	Undetermined	17.4	12.8

	M13- (Fg11)	Undetermined	17.3	13.0
	M14- (Fg11)	Undetermined	17.3	12.1
Keuper samples				
Rasquera	RA12	Miravet	14.9	16.6
Cabacés-Falset	K-1	El Molar	14.7	15.1
	K-2	El Molar	14.8	15.0
Gallicant	GA28	El Molar	15.0	16.5
	GA29	El Molar	14.8	15.8
Espinagosa	ES5	Miravet	15.1	12.9
	ES7	Miravet	15.4	13.8
	ES14	Miravet	15.3	12.7
	ES22	El Molar	14.6	13.5
	ES24	El Molar	14.2	12.6
Corbera	CO3	Miravet	15.4	11.3
	CO16	Miravet	15.3	11.9
	CO23	El Molar	14.5	14.1
Montgat	MG-1	Miravet	15.4	11.6
	MG-3	Miravet	15.0	12.9

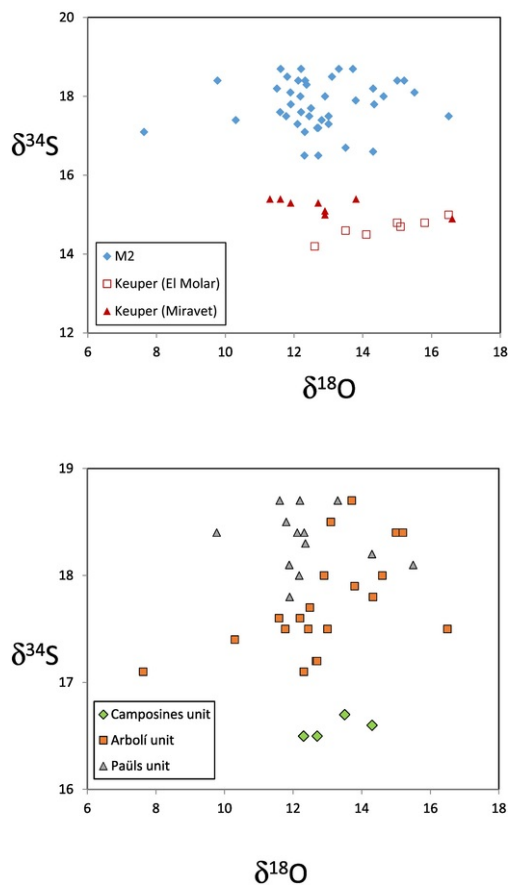


Fig. 9 Isotope composition of the sulfate ($\delta^{34}\text{S}$ and $\delta^{18}\text{O}$, in ‰) in the studied samples (gypsum and anhydrite). Upper figure: projection in which the values corresponding to the middle Muschelkalk and the Keuper units are distinguished. Lower figure: projection in which the values corresponding to the evaporite units of the middle Muschelkalk facies in the Catalan basin are distinguished.

alt-text: Fig. 9

The values obtained in the present study for the Keuper samples (secondary gypsum and anhydrite) of the Catalan basin range from 14.2 to 15.4‰ for $\delta^{34}\text{S}$, and from 11.3 to 16.6‰ for $\delta^{18}\text{O}$. (Table 4 and Fig. 9 upper part).

In the light of the foregoing data, the following aspects should be highlighted:

- 1) The $\delta^{34}\text{S}$ values for the middle Muschelkalk and for the Keuper samples form two distinct groups as shown in Fig. 9 (upper part). Thus, the sulfur isotope composition offers a geochemical criterion to distinguish the stratigraphic attribution of these Triassic evaporite units which commonly show very similar facies.
- 2) The $\delta^{34}\text{S}$ values of the samples of the middle Muschelkalk evaporite units (Fig. 9, lower part) show a slight decrease from the lower unit (Paüls ~~Gypsum~~ Gypsum unit) to the upper one (Camposines Gypsum unit) trending to values closer to those of the Keuper samples.
- 3) The most homogeneous values for $\delta^{34}\text{S}$, between 17.80 and 18.70‰, correspond to the lower evaporite unit (Paüls Gypsum unit). Moreover, the $\delta^{18}\text{O}$ values of this unit are very close in the samples of some outcrops (Paüls quarry, Pradell quarry, Vallirana mine; Table 4).
- 4) As for the Keuper values, it can be observed that the $\delta^{34}\text{S}$ values of the El Molar unit (upper Keuper), between 14.2 and 15‰, are slightly lower than those of the Miravet unit (lower Keuper), between 14.9 and 15.4‰ (Table 4 and Fig. 9 upper

part).

The sulfate isotope composition ($\delta^{34}\text{S}$ and $\delta^{18}\text{O}$) and the strontium isotope ratio ($^{87}\text{Sr}/^{86}\text{Sr}$) are the most commonly used geochemical proxies to determine (1) the origin, marine or non-marine, of the mother brines of the evaporitic sulfates, and (2) the contribution of different water sources to the evaporitic basins. The isotope composition of the dissolved marine sulfate has changed over time because of variations in the global sulfur cycle. These variations are reflected in the age curves of sulfur and oxygen isotopes in seawater sulfate (Claypool et al., 1980; Burke et al., 1982; Korte et al., 2003; Wortmann and Paytan, 2012). Based on these changes, the sulfate isotope composition of the evaporitic sulfates may also indicate their age (Utrilla et al., 1992; Bernasconi et al., 2017).

Throughout the Triassic, the marine sulfate isotope composition underwent marked and rapid variations following an extreme shift to heavier values at the onset of the Early Triassic. These fluctuations have been interpreted as related to the end-Permian mass extinction. This large biotic crisis disrupted the marine environmental conditions (widespread anoxia in the world's ocean) and severely interfered with the marine sulfur cycle which is linked to the carbon and oxygen cycles (Song et al., 2014; Bernasconi et al., 2017).

Until recently, $\delta^{34}\text{S}$ data for the Middle Triassic marine sulfates were scarce. Some values reported for the Iberian Peninsula can be found in Morad et al. (1995), Ortí et al. (1996) and Ortí et al. (2014) but the stratigraphic allocation of the samples analysed in these works is imprecise in some cases.

The recent paper by Bernasconi et al. (2017) provides new $\delta^{34}\text{S}$ data from marine sulfates ranging between the latest Permian to the Late Triassic from Northern Switzerland, and also data from marine sulfates in the western Tethys realm. The values reported by these authors for $\delta^{34}\text{S}$ of the Middle Muschelkalk (Anhydritgruppe) range from 19.0‰ to 21.8‰. However, values reported for the Keuper sulfates (Gipskeuper) are isotopically lighter ranging from 14.0‰ to 17.9‰ (Bernasconi et al., 2017, Supplemental data).

Although the isotope values obtained in the present work are lighter than those reported by Bernasconi et al. (2017) for the middle Muschelkalk and for the Keuper samples, the set of values reported in both studies allow us to clearly distinguish the sulfate units of the middle Muschelkalk from those of the Keuper in the respective basins. This is crucial not only when establishing the correct Triassic stratigraphic successions in the Catalan basin but also when it comes to solving structural issues as shown in works of regional geology in other Triassic basins of the Iberian peninsula (Boulouard and Viallard, 1981, in the Castillian Branch of the Iberian Ranges).

7.7 Siliciclastic facies associated with the evaporites

Compositional data of the fine to medium-grained sandstones forming the siliciclastic sediments in the middle Muschelkalk facies of the CCR are found in Virgili (1958), Cabañeros and Masriera (1977), Castellort (1986), and Morad et al. (1995). Virgili (1958) described the sandstones as quartzarenites and distinguished in these sandstones a metamorphic association of heavy minerals (staurolite, distene, andalucite) that is practically absent in the sandstones of the Buntsandstein facies. Cabañeros and Masriera (1977) identified in the sandstones the following minerals in decreasing order of abundance: quartz, feldspars, micas (muscovite, biotite and chlorite), and zircon and tourmaline as heavy minerals. The sandstone matrix was clayey and the cement carbonatic. Castellort (1986) documented the plagioclase-rich arkosic and subarkosic character of these sandstones, and assigned a granitic provenance to them. Morad et al. (1995) described the sandstones as subarkoses, arkoses and lithic subarkoses and lithic arkoses. The framework grains were predominantly quartz (25–70% in vol), K-feldspar (5–30%), rock fragments (2–20%), and muscovite (trace to 8%). These authors also documented in detail many diagenetic aspects of these deposits.

The source area of the siliciclastic materials of the middle Muschelkalk facies in the CCR has not been clearly established. Virgili (1985, 1958) suggested the possibility of a southern provenance for the siliciclastics of both the Buntsandstein and the middle Muschelkalk facies in the area of the Llobregat river. This interpretation was based on the anomalous thickness of the Buntsandstein conglomerates in that area. Castellort (1986) assumed a northern provenance (Montseny Massif), although variable in a fan of 90° (NW/NE-SE/SW). Transport distances from this source were estimated in about 50 km.

The siliciclastic deposits of the Guanta Sandstone unit of the middle Muschelkalk facies in the CCR are studied in the present paper only from a sedimentologic (environments and paleocurrents) point of view in order to refine the sandstone provenance. Three siliciclastic-dominated sections were studied in detail (Fig. 4; location in Fig. 2). Representations of the sandstone intervals in these sections (the Guanta Sandstone unit) are shown in Fig. 10. Each one of these intervals consists of a variable number of finning and thinning cycles of mudstones (mainly silts) and fine sandstones, which range from 1.5 to >10 m in thickness. Paleocurrent data collected from the three sections under study show rose diagrams of sole scouring ranging from N-275 to N-300 directions in the central part of the CCR, and of parting lineation and sole scouring ranging from N-310 to N-030 in the northern part. Current ripple crests, which show directions from N-035 to N-080, and N-090 to N-110 for the same parts, allow us to establish the flow sense. Additional descriptions of the three siliciclastic sections and their depositional cycles are shown in Table 5.

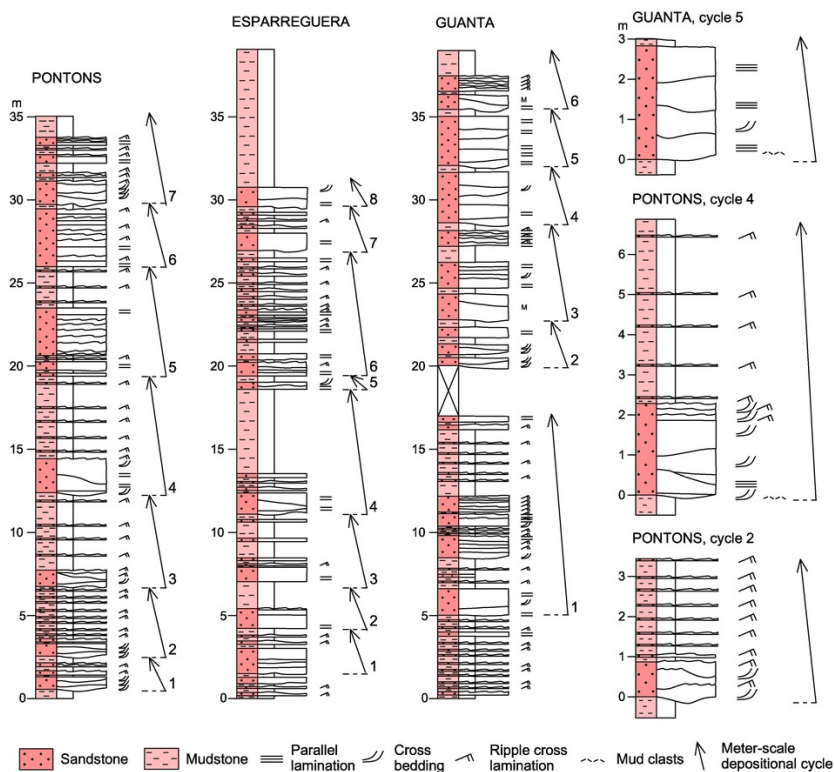


Fig. 10 Detailed stratigraphic intervals of the Guanta Sandstone unit in the Pontons, Esparreguera and Guanta sections. The unit thickness ranges between 30 and 35 m. The intervals are made of meter-scale finning and thinning upwards cycles. The most proximal cycles consist of erosive multistorey sandstone bodies composed of flat beds with parallel lamination and cross bedding with cross lamination, alternating upper flow regime and low flow regime deposit, depending on the episode. These sandstone bodies (cycle 4 in the Pontons section; cycles 2 and 3 in the Esparreguera section; cycles 4 and 5 in the Guanta section) are attributed to sandy midfan distributive channels. Apart from the basal sandstone bodies, flat beds with parallel lamination up to 1 m thick can appear (cycle 1 in the Guanta section), corresponding to flood flows spreading from channels. These flows are shallow, prevailing upper flow regime. More distally distributive channels (cycles 1, 2, and 3 in the Pontons section) can be found below and above the most proximal cycles; these deposits are formed in low flow regime. Sections location in [Fig. 2](#).

alt-text: Fig. 10

Table 5 Descriptions of the siliciclastic deposits (Guanta Sandstone unit) of the middle Muschelkalk facies in the Triassic Catalan basin. Stratigraphic sections: Pontons, Esparreguera and Guanta ([Fig. 10](#)). Location of these sections in [Fig. 2](#). DC: depositional mudstone-sandstone cycle.

alt-text: Table 5

<p><i>General observations:</i> The beds from the sandstone bodies range from centimeters to one-1 meter in thickness and bedding can be parallel and non-parallel. Composite interbedded sandy siltstones and silty mudstones form the upper part of the cycles. Sole surfaces in the cycles are erosive and most of them are planar. Only occasionally is the sole erosion due to scouring.</p>
<p>Pontons section (51 m thick)</p>
<p>- <i>Hydraulic regime:</i> low and upper flow regime;</p>
<p>- <i>Finning and thinning upwards cycles:</i> there are 7 cycles, with single thickness from 1.5 to 7 m.</p>
<p>- <i>Basal sandstone bodies:</i> these bodies are multistorey in all the cycles, combining non-parallel bedding with cross-lamination and flat bedding with parallel lamination;</p>
<p>- <i>Thickest cycle:</i> it is number 4, of 7 m in thickness. The basal sandstone body of this cycle is 2.2 m thick, and it is made up of 5 beds from 0.2 to 1 m thick; in the two lower beds, cross-lamination and parallel lamination alternate, while cross lamination is present in the upper bed; a 0.6 m thick layer with cross and ripple lamination forms the top of the sandstone body. This basal sandstone body has a lateral extension of</p>

about 65 m; ~~whitin~~**within** this body, the lateral extension of the channel shoal bedding is 20 m; this body combines upper and low flow regime sedimentary structures and corresponds to a midfan distributive channel. This cycle is the most proximal facies of the Pontons section;

- *Other cycles*: the three lower cycles (DC1 to 3) have basal sandstone bodies of <1 m thick, which are multistorey and have channel-shaped bedding and cross lamination. In DC2, the lateral extension of the basal sandstone body is 22 m. These three lower cycles show flow regime and correspond to distal fan distributive channels. DC5 and DC6 bear thicker multistorey basal sandstone bodies but they are made up of thinner beds with irregular and curved bounds; sedimentary structures appear less manifest in these cycles. DC6 corresponds to a midfan distributive channel. DC7 has the same characteristics as the three lower ones, with a multistorey sandstone body of 1 m thick that shows lenticular bedding;

- *Paleocurrent directions*: they are N-275 to N-305 from current scour marks, and N-305 to N-350 from the crests of the current ripples. In the cycles these directions are as follows: in DC1: scour N-305, and current ripples N-305/330/350; in DC2: scour N-275; in DC4: scour N-300; in DC7: scour N-285.

Esparreguera section (70 m thick)

- *Hydraulic regime*: low and upper flow regime;

- *Finning and thinning upwards cycles*: there are 8 cycles, with single thickness from 2 to 8 m.

- *Thickest cycle*: it is number 4, of 8 m in thickness;

- *Thickest sandstone body*: it is 1.8 m thick, in cycle number 1. Laterally, however, it is up to 3 m thick, multistorey and made up of beds up to 1.3 m thick and with a lateral extensions of about 20 m, which together build a sandstone body of at least 120 m of lateral extension. Bedding shows parallel and cross-lamination. A remarkable feature is the presence of a cross-lamination set superimposed on a parallel lamination set in the same bed;

- *Other basal sandstone bodies*: the basal sandstone bodies of the other cycles are multistorey, combining tabular bedding with parallel lamination and cross-bedding with cross lamination. The thickness is 1 m or less. Locally, mud clasts appear at the sandstone bodies' sole, or even at internal bounding surfaces. Sets and cosets of ripple lamination form the top of the sandstone bodies and are interbedded in the upper part of the cycles. DC1 is the most proximal cycle. DC2 shows gradation from less important midfan distributive channel to distal distributive one;

- *Paleocurrent directions*: in DC1 (the thickest sandstone body) they are N-345, N-355 and N-340 from current scour marks and parting lineation, and flow direction and sense from N-90 to N-110 from straight current ripples; in DC3: N-340 from parting lineations; in DC6: N-05 from scour; in DC8: N-15 from scours.

Guanta section (68 m thick; the base and the top of this sections do not croup out)

- *Hydraulic regime*: low and upper regime. This is the most proximal of the three sections studied;

- *Finning and thinning upwards cycles*: there are 5 cycles;

- *Thickest cycle*: it is number 2. Its basal sandstone body is 1.5 m thick, with lateral length of 30 m.

- *Other cycles*: The other three cycles exhibit thicker basal sandstone bodies, reaching up to 5 m. These sandstone bodies are made up of beds ranging from 0.2 to 1 m in thickness. Bedding shows cross lamination as well as parallel lamination, even the two types in the same bed laterally. Occasionally, a set or a coset of ripple bedding forms the top of the beds. The lateral extension of the thickest beds reaches 12 m (in DC4) and 15 m (in DC5). Mud clasts can appear at the sole of the sandstone bodies, or even at any internal bonding surface. The DC3 shows low flow regime grading upwards to upper flow regime. In DC4 the possible lateral extent of the channel (basal sandstone body) is >100 m;

- *Paleocurrent directions*: in DC2: N-335 from scour marks and N-310 from parting lineation; in DC4: N-030 from scour marks.

~~7.1.~~**7.1 Interpretation**

The mudstone-sandstone cycles forming the Guanta Sandstone unit are interpreted as the sedimentary product of midfan distributive channels and floodplains of ephemeral streams in sandy alluvial fans. As a whole, these cycles were sedimented in an alluvial plain. All the paleocurrent data, roughly coming from the NW ([Table 5](#)), suggest provenance from the Lleida High, located to the W and NW of the basin ([Fig. 1A](#)). In fact, these paleocurrent data are not very different from those documented for the sandstones of the Buntsandstein facies in [Marzo \(1980\)](#) and in [Calvet and Marzo \(1994\)](#).

~~8.~~**8 Discussion**

~~8.1.~~**8.1 Evaporitic evolution of the basin**

The section correlation profile ([Fig. 4](#)) allow us to propose a first approach to the tridimensional framework of the middle Muschelkalk facies in the Triassic Catalan basin before its re-structuration during the Alpine orogeny ([Fig. 11](#)). The three evaporite units distinguished by us in this facies suggest that the platform restriction was continuous during the whole sedimentation period. Moreover, the higher thickness of the evaporite units towards the SW of the basin together with their lateral gradation into siliciclastics towards the NE indicate that structural factors controlled the sedimentation in the basin.

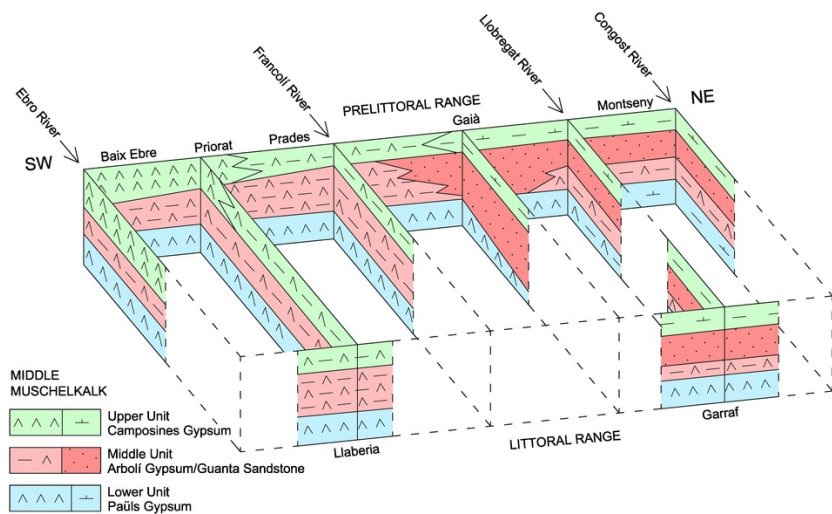


Fig. 11 Stratigraphic framework for the middle Muschelkalk facies in the Triassic Catalan basin. The most significant lateral facies changes are indicated. Scheme out of scale.

alt-text: Fig. 11

8.1.1.8.1.1 Lower Unit: transgressive sulfate lagoon

Within this basinal unit, the Paüls Gypsum unit occurred after the abrupt end of the sedimentation of the lower Muschelkalk carbonates. Thereafter, massive precipitation of sulfate occurred throughout the platform in a wide lagoonal setting (Fig. 12). Similar sulfate lagoons are known to have occurred in other evaporitic basins of the eastern Iberian platform during the Middle Triassic-Lower Jurassic period just at moments of rapid environmental change from carbonate to sulfate precipitation (Ortí et al., 2017). These sulfate lagoons were characterized by (1) very high proportion of calcium sulfates; (2) scarcity of chlorides (Iberian basin; Suárez Alba, 2007) or even total absence of them (Ebro basin; Gómez et al., 2007); (3) association with variable or even very small amounts of carbonates; (4) variable record of depositional cyclicity; and (5) relative platform uniformity at that time. In the case of the Paüls Gypsum unit of the Catalan basin, carbonate is scarce and cyclicity is recorded only locally in the lower part of the unit. The sulfates extended throughout a uniform lagoonal basin, although mudstones were predominant in the northeastern part.

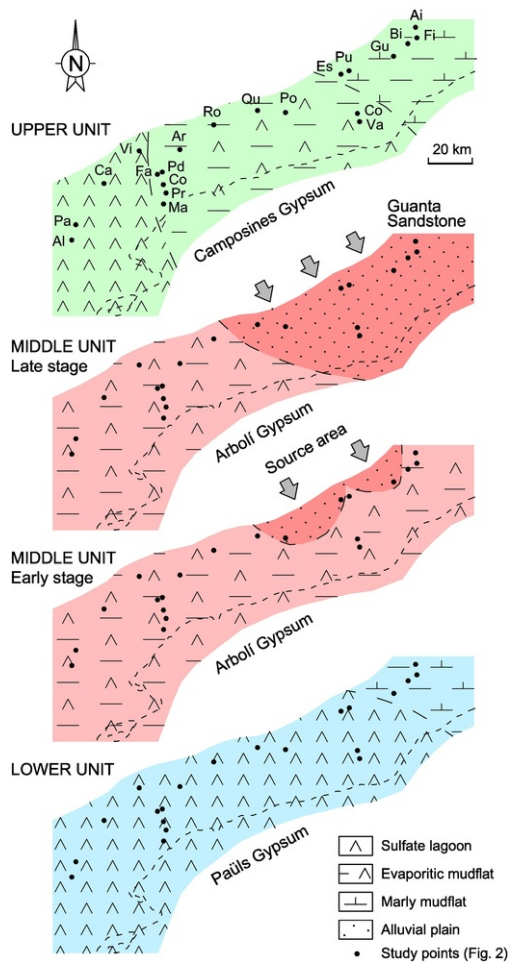


Fig. 12 Schematic diagrams of the evaporitic evolution of the middle Muschelkalk facies in the Triassic Catalan basin. The most significant environments are indicated. Units from base to top: Lower Unit, including the Paüls Gypsum unit (transgressive sulfate lagoon); Middle Unit, including the Arbolí Gypsum unit and the Guanta Sandstone unit (regressive evaporitic mudflat-alluvial plain). An early stage is distinguished from a late one in the development of the siliciclastic facies; Upper Unit, including the Camposines Gypsum unit (transgressive sulfate lagoon-evaporitic mudflat).

alt-text: Fig. 12

The sharp carbonate-to-sulfate change at the top of the lower Muschelkalk unit in the Catalan basin is of special interest. The top of this unit shows a 1 m thick carbonate bed affected by marked undulation, resembling stromatolites (Fig. 6A, B), and also exhibits ferruginous and karstic features locally. This bed has been interpreted by Esteban et al. (1977) as equivalent to the shallow subaqueous carbonate crusts which are currently forming in Bahamas and Florida. The same carbonate bed has been interpreted by Calvet and Marzo (1994) as a laminated calcrete with supratidal tepees, stromatolites and breccias. Accordingly, the laminated sulfates of the overlying Paüls Gypsum unit can be interpreted as deposited in a water body significantly deeper than that of the top carbonate crust. The relative water rise associated with this transgressive trend could occur under structural or merely eustatic controls, or both. Given the combination of a sudden basinal restriction and a deeper-water setting, we may interpret that an extensional pulse provoked the basin confinement and prevented the carbonate production in a relatively uniform platform. Intense deposition of evaporites occurred in the south of the basin.

8.1.2.8.1.2 Middle Unit: regressive evaporitic mudflat-alluvial plain

Within this basinal unit, sedimentation occurred in two differentiated areas. In the southern and eastern parts of the basin, the evaporitic deposition continued as an alternation of red mudstone beds and gypsum beds (Arbolí Gypsum unit, Fig. 12).

This alternation indicates the rapid change from the preexistent sulfate lagoon into a wide evaporitic mudflat colonised by a dense net of shallow salinas surrounded by sabkhas (gypsum-anhydrite bodies). Depositional cyclicity in this evaporitic mudflat occurred almost permanently. This red mudstone-gypsum alternation is very similar to those present in other Triassic basins of Iberia in both the Keuper and the middle Muschelkalk successions, whose depositional setting has been called ‘clay-gypsum alternation salinas’ in [Ortí et al. \(2017\)](#).

Some areas of the northeastern half of the Catalan basin received important inputs of fine to medium-grained siliciclastics (Guanta Sandstone unit). Most probably these materials came from the Lleida High located to the W and NW of the study area, which would have undergone uplift at that time ([Fig. 12](#)). In an early stage, the inputs were limited to the NW area of the basin, but they expanded largely to the SE in a later stage. These materials were accumulated as fans in alluvial plains, where they prevented the local precipitation of evaporites. The precise sedimentological relationships between the meter-scale cycles recorded in the Arbolí Gypsum unit ([Fig. 5](#)) and in the Guanta Sandstone unit ([Fig. 10](#)) remain unclear. Probably the dynamics of the alluvial fan systems induced shifting in the frontal and peripheral salinas, which hinders the cycle correlation between them.

As a whole, an evaporitic mudflat (Arbolí Gypsum)-alluvial plain (Guanta Sandstones) complex occupied the basin during most of the Middle Unit time. This complex recorded the maximum sediment accumulation of the middle Muschelkalk facies, suggesting the maximum extensional activity in the platform. Towards the top of this complex, however, the predominance of red mudstones at basin scale suggests deceleration of the activity. This deceleration led to final exposure conditions in a wide, distal red mudflat. Compared to the Lower Unit, the Middle Unit represents regressive trend, progressive loss of marine influence, and lack of uniformity in the depositional environments of the basin.

~~8.1.3.~~~~8.1.3~~ ***Upper Unit: transgressive sulfate lagoon-evaporitic mudflat***

Overlying the Middle Unit, the lithologic assemblage formed by the evaporites, marls, carbonates, and variegated mudstones of the Upper Unit was deposited. This lithologic change was gradual and suggests a new marine flooding in the basin and a transgressive trend in the sediments. The progressive lateral gradation from (a) marls, carbonates and variegated mudstones in the absence of evaporites in the northern part of the basin into (b) evaporites, variegated mudstones, marls, and carbonates in the central part (evaporitic mudflat), and into (c) the Camposines Gypsum unit (sulfate lagoon) in the southern part represents the evolution, in the same direction, from a marly mudflat into a sulfate lagoon (Camposines Gypsum unit) ([Fig. 12](#)). The significant thickness difference between the sediments of the marly mudflat (5–15 m) and the sulfate lagoon (up to 60 m) indicates fault control on the sedimentation presumably linked to a new extensional pulse. In fact, a transgressive trend towards the west had been already assumed by Castelltort (in [Marzo and Calvet, 1985](#)) for its upper basinal unit. This transgressive Upper Unit graded upwards into the marine carbonates of the upper Muschelkalk.

~~8.2.~~~~8.2~~ **Comparison with the Triassic Maestrat basin**

The Triassic Maestrat basin was a very subsident area that accumulated about 1500 m of Triassic sediments, most of them evaporites. Towards the southwest ([Fig. 1A](#)), this basin was separated from the wider Triassic Iberian basin by the NW-SE elongated Ateca-Castellón High ([Castillo Herrador, 1974](#)). Towards the northeast, the basin was connected to the Triassic Catalan basin.

The evaporitic successions of the middle Muschelkalk facies in the Catalan basin can be compared to the corresponding one in the adjacent Triassic Maestrat basin. In the Maestrat basin, this evaporitic succession, which is very rich in chlorides and sulfates, is only known thanks to deep boreholes ([Bartrina and Hernández, 1990](#)) ([Fig. 13](#)). In some of these boreholes such as the Bobalar-1 and Bobalar-2, the evaporitic succession shows structural deformation of a diapiric origin, attaining 1000 m in thickness. Isotopic values of four anhydrite samples in this succession obtained for the present paper in the Bobalar-1 borehole ([Table 4](#), [Fig. 9](#) upper part) are consistent with the values obtained in the middle Muschelkalk sulfates of the Catalan basin.

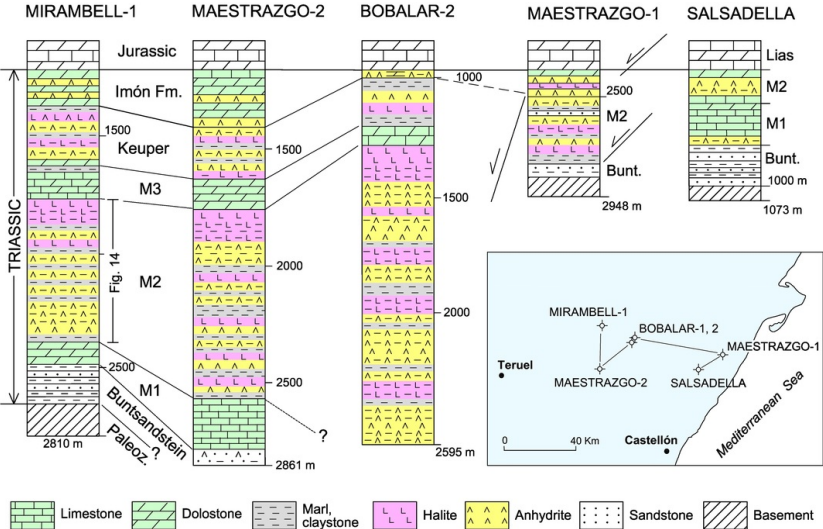


Fig. 13 Correlation profile of deep boreholes in the Triassic Maestrat basin. Modified from Bartrina and Hernández (1990, fig. 1). The anomalous thickness of the middle Muschelkalk interval in the Maestrazgo-2 and the Bobalar-2 boreholes is due to salt tectonics.

alt-text: Fig. 13

Other boreholes in the Triassic Maestrat basin, however, show undisturbed successions, indicating preservation of the depositional thickness and the bedding geometry. This is the case of the Mirambell-1 borehole, which intersects a horizontal succession of the middle Muschelkalk facies that attains 625 m in thickness. At present, a possible correlation between this succession and the one in the Catalan basin could be based (1) on the original lithologic description of the Mirambell-1 borehole (internal report of Auxini, 1974) (Table 6), and (2) on the subsurface distribution of the middle Muschelkalk facies in the Maestrat basin deduced from seismic profiles, which has been recently documented by Nebot and Guimerà (2016a, 2016b).

Table 6 Lithologic description for depth intervals of the Mirambell-1 deep borehole (Auxini, 1974) (no mention to the 1842–1848 m interval is found in the original description).

alt-text: Table 6

Mirambell-1 deep borehole (Auxini, 1974)
Middle Muschelkalk: 1774–2398 m (624 m):
- 1774–1842 m: Halite rock, translucent and bearing thicker horizons of greenish-gray claystone;
- 1848–1889 m: Beige claystone with levels of gray claystone;
- 1901–1938 m: Anhydrite, salt rock, and plastic gray claystone;
- 1938–2004 m: Plastic gray claystone with some levels of anhydrite and salt;
- 2004–2030 m: Salt rock with thin levels of claystone;
- 2030–2248 m: Irregular alternation of beige anhydrite, salt with clayey-anhydritic inclusions, and plastic, green-gray claystone;
- 2248–2266 m: Massive, white salt rock;
- 2266–2352 m: Hard, saliferous-anhydritic gray claystone; compact, severely recrystallized anhydrite bearing intercalations of dolomitic claystone;
- 2352–2362 m: Slightly dolomitic, gray marls;
- 2362–2378 m: Hard, recrystallized beige anhydrite with some levels of dolomitic claystone;
- 2378–2392 m: Salt rock with anhydrite at the base;

- 2392-2398 m: Pastry beige, calcareous dolostone with anhydrite inclusions.

As regards the Mirambell-1 borehole succession, our graphic version of the lithologic description by [Auxini \(1974\)](#) is shown in [Fig. 14](#). The thick evaporitic-siliciclastic interval in the middle of the succession (2030-2248 m: Irregular alternation of beige anhydrite, salt with clayey-anhydritic inclusions, and plastic, green-gray claystone; [Table 5](#)) seems to be equivalent to the Arboli Gypsum unit of the Catalan basin. This interval also seems to divide the succession into three evaporitic intervals. As for the distribution of the middle Muschelkalk facies across the basin based on seismic profiles, [Nebot and Guimerà \(2016a, 2016b\)](#) have distinguished a thicker lower part from a thinner upper part, the upper part being markedly expansive with respect to the lower one. The lower part is interpreted as the sediment fill of very subsiding zones generated by a pulse of extensional reactivation ([Fig. 14](#)), which occurred after the sedimentation of the lower Muschelkalk carbonates. The upper part is interpreted as the result of the attenuation of the extensional activity leading to expansion of the depositional area and to uniformity of the sedimentation at basin scale ([Nebot and Guimerà, 2016a, 2016b](#)).

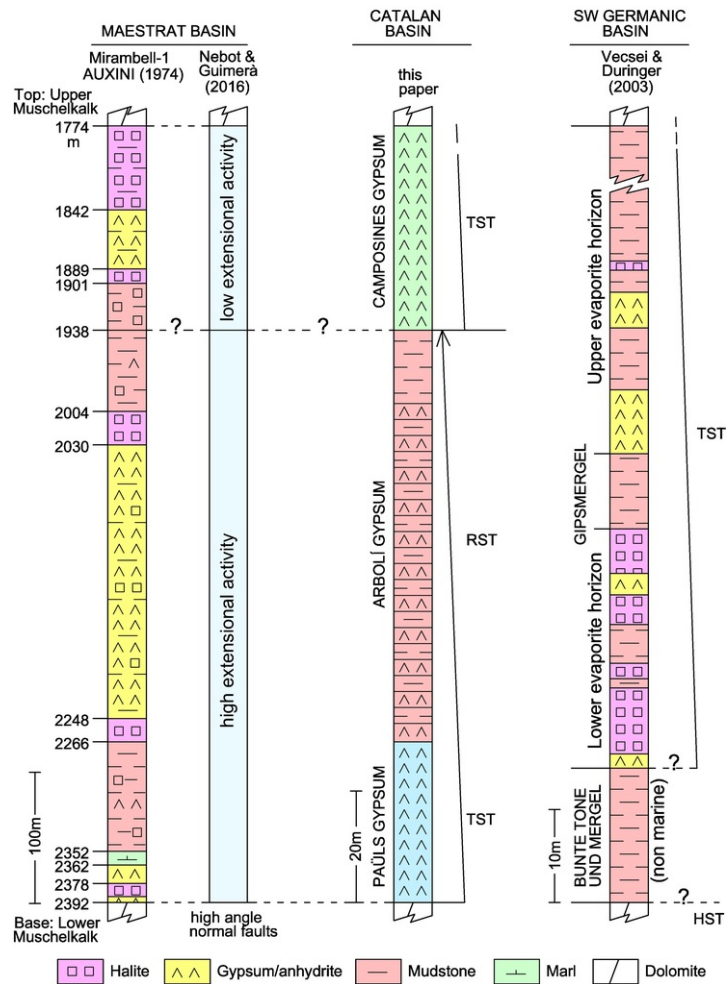


Fig. 14 Comparison of middle Muschelkalk facies in the Triassic Maestrat and Catalan basins. Note the different thickness scales. Left: Maestrat basin. Middle Muschelkalk succession in the Mirambell-1 deep borehole (adapted in this work from data in [Table 6](#)). The tentative correlation of this succession with the two structural parts identified at basin scale by [Nebot and Guimerà \(2016a, 2016b\)](#) is indicated. Centre: Catalan basin. Succession type in the evaporite-rich, southern part of the basin. The deduced (this paper) episodes of transgression or regression are shown. Right: SW Germanic basin (after [Vecsei and Düringer, 2003](#)). Sarreburg succession (modified and adapted from fig. 4 of [Vecsei and Düringer, 2003](#)). Note the interpretation of the whole marine part (Gypsmergel) of this Middle Muschelkalk succession as a transgressive system tract.

Accordingly, it can be interpreted that the three deduced intervals in the Mirambell-1 borehole could be roughly equivalent to the three basal units in the Catalan succession, respectively (Fig. 14). The change in the extensional activity documented by Nebot and Guimerà (2016a, 2016b) in the Maestrat basin could be correlated to the change from the regressive trend (Arbolí Gypsum unit) to the transgressive one (Camposines Gypsum unit) interpreted by us in the Catalan basin (Fig. 14).

The former interpretation suggests the lateral continuity between the two basins, at least during the middle Muschelkalk time interval. Apparently, the presence (Maestrat basin) or practical absence (Catalan basin) of chloride bodies could be a marked difference between the two basins. However, if a lateral continuity is assumed, these bodies in the Maestrat basin could derive from the post-sulfate brines drained-off from the adjacent Catalan basin, where only sulfates precipitated. The higher subsidence rate in the Maestrat basin at that time would have favored this flow of heavy brines.

As for the continuity of the middle Muschelkalk succession of the Triassic Catalan basin towards the east (underneath the Mediterranean Sea), little documentation is available. The offshore Tarragona D-1 deep borehole - located to about 50 km to the east of the present day coastal line at a latitude intermediate between the Ebro Delta and the Tarragona city-, drilled 89 m of a middle Muschelkalk succession formed by mudstones and anhydrite. This succession is intercalated between a 58 m thick interval of lower Muschelkalk dolostones and a 98.5 m thick interval of upper Muschelkalk dolostones (Lanaja, 1987). This offshore stratigraphic record suggests the continuity to the east of the middle Muschelkalk evaporites.

8.3.8.3 Third-order depositional sequences

In NE Iberia, the detrital-evaporitic sediments of the middle Muschelkalk facies occupy different positions in the various proposals of third-order depositional sequences, depending on the authors (Fig. 15). Some papers consider that (1) the first marine (eustatic or tectono-eustatic) transgression during the Triassic was formed by the Rôt facies at the base and the lower Muschelkalk facies at the top, and (2) that the second transgression was formed by the middle Muschelkalk facies at the base and the upper Muschelkalk facies at the top. The two transgressions constituted third-order depositional sequences (Calvet et al., 1990; López-Gómez et al., 1998). The interpretations of the middle Muschelkalk facies in the Iberian and Catalan basins usually have associated this facies with regressive trends and with lowstand positions of the sea level. These interpretations also have considered that this facies is included in a single, third-order sequence in association with the upper Muschelkalk carbonates (López-Gómez and Arche, 1994; Suárez Alba, 2007; among others) (Fig. 15). Some papers have also identified an erosive, unconformable boundary between this facies and the underlying lower Muschelkalk carbonates (López-Gómez and Arche, 1992; Calvet and Marzo, 1994) or their equivalent terrigenous facies near the border of the Iberian Massif to the west (García-Gil, 1990, 1994).

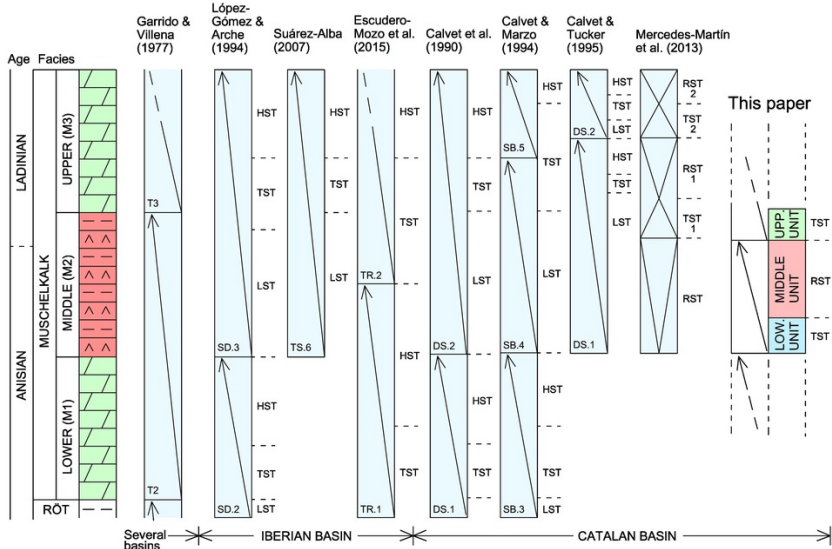


Fig. 15 Third-order depositional sequences (arrows) in the Muschelkalk facies as assumed by several authors in some Triassic basins of NE Iberia. The proposal of modification for the middle Muschelkalk facies in the Catalan basin is indicated. The assemblage of the Lower Unit (TST) and the Middle Unit (RST) is considered to be an independent, third-order depositional sequence.

In contrast, other authors have separated the detrital-evaporitic middle Muschelkalk facies into two different third-order sequences. This is the case of [Escudero-Mozo et al. \(2015\)](#), in which a lower part of the middle Muschelkalk facies in the Iberian basin is located at the top of the first marine sequence (TR1 sequence), whereas an upper part is located at the base of the second marine one (TR2 sequence) ([Fig. 15](#)). This is also the interpretation by [Mercedes-Martín et al. \(2013\)](#) in the Catalan basin, who divided the middle Muschelkalk facies into two different third-order depositional sequences ([Fig. 15](#)). The stratigraphic intervals in which the middle Muschelkalk facies is divided are ambiguous in these interpretations. However, the middle Muschelkalk succession in the Triassic Catalan basin might shed some light on this ambiguity.

In the Catalan succession, the assemblage of the transgressive Lower Unit and the regressive Middle Unit could be considered as an independent, third-order depositional sequence. The thickness of this sequence varies between 50 and 100 m on the surface, although in the subsurface the thickness could be higher due to evaporite preservation from possible surface dissolution. Moreover, the transgressive Upper Unit would represent the base of the overlying third-order sequence, and the upper part of this sequence would be formed by the carbonates of the upper Muschelkalk facies ([Fig. 15](#)). In fact, a transgressive trend in the upper part of the middle Muschelkalk succession had been already assumed by [Mercedes-Martín et al. \(2013\)](#) for the Triassic Catalan basin ([Fig. 15](#), TST-1).

In other basins, some authors have interpreted the middle Muschelkalk facies as transgressive. This is the case of [Vecsei and Düringer \(2003\)](#) in the SW Germanic basin ([Fig. 14](#)). The following features of this Middle Muschelkalk succession should be highlighted: (a) the presence of two evaporite units, the lower one with chlorides (halite) and anhydrite, and the upper one mainly with anhydrite; (b) the presence of cycles with ‘upwards-increasing terrigenous content’ (decreasing-upwards salinity cycles); and (c) the consideration of transgressive system tract for the entire marine interval of the succession which overlies the basal, non-marine ‘Bunte Tone und Mergel’ unit.

9.9 Conclusions

The presence of three lithostratigraphic units at basin scale (Lower, Middle and Upper) in the detrital-evaporitic middle Muschelkalk succession of the Triassic Catalan basin is corroborated. Moreover, each one of these basinal units includes a distinct evaporite unit. In all of these units, the isotopic values of gypsum samples, which are very homogeneous, indicate the marine origin of the mother brines. These values also allow a clear distinction from those of the Keuper sulfates in this basin.

The characterization of the three evaporite units contributes to our understanding of the evolution and tectonic activity in the basin. The Paüls Gypsum unit (in the Lower Unit) involves a sharp environmental change from the very shallow platform carbonates at the top of the lower Muschelkalk facies to the laminated sulfates of a widespread, deeper lagoon. This transgression was probably linked to an extensional pulse affecting the northeastern sector of the Iberian platform during the Anisian (Middle Triassic).

On the preexistent lagoon, the Arbolí Gypsum unit (in the Middle Unit) represents the generalised development of a regressive evaporitic mudflat, which was formed by a mosaic of shallow gypsum salinas surrounded by anhydrite sabkhas. This mudflat graded laterally into the alluvial plain of the Guanta Sandstone unit, which occupied several areas in the central and northern parts of the basin. The most probable provenance of the fine to medium-grained siliciclastics is from the Lleida High, located to the W and NW, which would have undergone uplift at that time. This provenance is useful for delineating the western boundary of the basin.

The Camposines Gypsum unit (in the Upper Unit) represents a new marine flooding, although the evaporite precipitation was limited to the southern and central parts of the basin. As a whole, the Upper Unit means a transgressive trend probably linked to a new pulse of extensional activity in the northeastern sector of the Iberian platform. This pulse resulted in the end of the basin restriction and in the generalisation of the upper Muschelkalk carbonates.

The evaporitic succession of the middle Muschelkalk facies in the Triassic Catalan basin seems to be correlatable with the coeval and thicker succession recorded in the adjacent Triassic Maestrat basin in which evaporites are totally predominant.

In the Triassic Catalan basin, the possibility of considering the assemblage of the Lower Unit and the Middle Unit as a third-order, single sequence is proposed. The Upper Unit would be the base of the overlying sequence, whose top would be the upper Muschelkalk carbonates.

Uncited reference

[Garrido and Villena, 1977](#)

Acknowledgements

This study was supported by research projects 2009 SGR1451 (Departament d’Innovació, Universitats i Empresa) and 2017 SGR824 (Agència de Gestió d’Ajuts Universitaris i de Recerca) of the Catalan Government and CGL2015-66835-P of the Spanish Government (Ministerio de Ciencia e Innovación). [Review comments by Editor Prof. Brian Jones and two anonymous reviewers improved the manuscript.](#)

References

- Auxini, Informe final del sondeo MIRAMBELL-1. Departamento de Investigaciones Petrolíferas, Inf. 08491, In: *Technical Report*, 1974, Auxini; Madrid, 1-35.
- Bartrina T. and Hernández E., Las unidades evaporíticas del Triásico del subsuelo del Maestrazgo, In: Ortí F. and Salvany J.M., (Eds.), *Formaciones Evaporíticas de la Cuenca del Ebro y Cadenas periféricas, y de la Zona de Levante*, 1990, ENRESA-Universitat de Barcelona, 34-38.
- Bernasconi S.M., Meier I., Wholwend S., Brack P., Hochuli P.A., Bläsi H., Wortmann U.G. and Ramseyer K., An evaporite-based high-resolution sulfur isotope record of the Late Permian and Triassic seawater sulfate, *Geochimica et Cosmochimica Acta* **204**, 2017, 331-349.
- Boulouard C. and Viallard P., Identification du Ladinien et du Carnien dans les marnes triasiques de la Serranía de Cuenca (Chaîne Ibérique sud occidentale, Espagne): Considérations stratigraphiques et structurales, *Bulletin des Centres de Recherches Exploration-Production Elf-Aquitaine* **5**, 1981, 31-41.
- Burke W.H., Denison R.E., Hetherington E.A., Koepnick R.B., Nelson H.F. and Otto J.B., Variation of seawater ⁸⁷Sr/⁸⁶Sr throughout Phanerozoic time, *Geology* **10**, 1982, 516-519.
- Cabañeros M.C. and Masriera A., Contribución al conocimiento sedimentológico del Muschelkalk medio de los Catalánides, *Cuadernos de Geología Ibérica* **14**, 1977, 149-156.
- Calvet F. and Marzo M., El Triásico de la Cordilleras Costero Catalanas: Estratigrafía, Sedimentología y Análisis Secuencial, In: *III Coloquio de Estratigrafía y Paleogeografía del Pérmico y Triásico de España, Cuenca, Field trip Guide*, 1994, 1-53.
- Calvet F. and Tucker M., Outer ramp cycles in the Upper Muschelkalk of the Catalan Basin, northeast Spain, *Sedimentary Geology* **57**, 1988, 185-198.
- Calvet F., Tucker M. and Henton J.M., Middle Triassic carbonate ramp systems in the Catalan Basin; northeast Spain: facies, system tracts, sequences and controls, In: Tucker M.E., et al., (Eds.), *Carbonate Platforms: Facies, Sequences and Evolution, Special Publication of the International Association of Sedimentologists* **9**, 1990, Blackwell Scientific Publications; Oxford, 79-108.
- Castelltort X., Estratigrafia del Muschelkalk mitjà dels Catalànids i Sedimentologia de les seves unitats detrítiques, (Graduate Thesis)1986, Universitat de Barcelona.
- Castillo Herrador F., Le Trias évaporitique des basins de la Vallée de l'Èbre et de Cuenca, *Bulletin de la Société Géologique de France* **16** (6), 1974, 666-675.
- Claypool G.E., Holser W.T., Kaplan I.R., Sakai H. and Zak I., The age curves of sulfur and oxygen isotopes in marine sulfate and their mutual interpretation, *Chemical Geology* **28**, 1980, 199-260.
- Escudero-Mozo M.J., Márquez-Aliaga A., Goy A., Martín-Chivelet J., López-Gómez J., Márquez L., Arche A., Plasencia P., Marzo M. and Sánchez-Fernández D., Middle Triassic carbonate platforms in eastern Iberia: evolution of the fauna and palaeogeographic significance in the western Tethys, *Palaeogeography, Palaeoclimatology, Palaeoecology* **417**, 2015, 236-260.
- Esteban M., Pomar L., Marzo M. and Anadón P., Naturaleza del contacto entre Muschelkalk inferior y Muschelkalk medio de la zona de Aiguafreda (Provincia de Barcelona), *Cuadernos de Geología Ibérica* **4**, 1977, 201-210.
- García-Gil S., Estudio sedimentológico y paleogeográfico del Triásico en el tercio noroccidental de la Cordillera Ibérica (provincias de Guadalajara y Soria), (Ph.D. Thesis)1990, Universidad Complutense de Madrid; Spain.
- García-Gil S., El Triásico de la región de Riba de Santiuste-Arcos de Jalón, In: *III Coloquio de Estratigrafía y Paleogeografía del Pérmico y Triásico de España, Cuenca, Field trip Guide*, 1994, 1-52.
- Garrido A. and Villena J., El Trias germánico en España: paleogeografía y estudio secuencial, *Cuadernos de Geología Ibérica* **4**, 1977, 37-56.
- Gómez J.J., Goy A. and Barrón E., Events around the Triassic-Jurassic boundary in northern and eastern Spain: a review, *Palaeogeography, Palaeoclimatology, Palaeoecology* **244**, 2007, 89-110.
- Korte Ch., Kozur H.W., Bruckschen P. and Veizer J., Strontium isotope evolution of Late Permian and Triassic seawater, *Geochimica et Cosmochimica Acta* **67**, 2003, 47-62.
- Lanaja J.M., Contribución de la Exploración Petrolífera al conocimiento de la Geología de España, 1987, Instituto Tecnológico GeoMinero de España; Madrid, 1-465.
- López-Gómez J. and Arche A., Las unidades litoestratigráficas del Pérmico y Triásico Inferior y Medio en el sector SE de la Cordillera Ibérica, *Estudios Geológicos* **48**, 1992, 123-143.
- López-Gómez J. and Arche A., El Triásico y Pérmico del SE de la Cordillera Ibérica, In: *III Coloquio de Estratigrafía y Paleogeografía del Pérmico y Triásico de España, Cuenca, Field trip Guide*, 1994, 1-70.

- López-Gómez J., Arche A., Calvet F. and Goy A., Epicontinental marine carbonate sediments of the Middle and Upper Triassic in the westernmost part of the Tethys Sea, Iberian Peninsula, *Zbl.-Geol.-Paläontol. Zentralblatt für Geologie und Paläontologie* **9-10**, 1998, 1033-1084.
- Marzo M., El Buntsandstein de los Catalánides: Estratigrafía y Procesos de Sedimentación, (Ph.D. Thesis)1980, Universitat de Barcelona; Spain.
- Marzo M. and Calvet F., Guía de la Excursión al Triásico de los Catalánides, In: *II Coloquio de Estratigrafía y Paleogeografía del Pérmico y Triásico de España, La Seu d'Urgell, Field trip Guide*, 1985, 1-175.
- Mercedes-Martín R., Salas R. and Arenas C., Facies heterogeneity and depositional models of a Ladinian (Middle Triassic) microbial-dominated carbonate ramp system (Catalan Coastal Ranges, NE Spain), *Marine and Petroleum Geology* **46**, 2013, 107-128.
- Mitjavila J. and Martí J., El volcanismo triásico del sur de Catalunya, *Revista de Investigaciones Geológicas de la Diputación Provincial de Barcelona* **42** (43), 1986, 89-103.
- Moore D. and Reynolds R.C., Jr, X-ray Diffraction and the Identification and Analysis of Clay Minerals, 1989, Oxford University Press; Oxford.
- Morad S., Al-Aasm I.S., Longstaffe F.J., Marfil R., De Ros L.F., Johansen H. and Marzo M., Diagenesis of a mixed siliciclastic/evaporitic sequence of the Middle Muschelkalk (Middle Triassic), the Catalan Coastal Range, NE Spain, *Sedimentology* **42**, 1995, 749-768.
- Nebot M. and Guimerà J., Structure of an inverted basin from subsurface and field data: the Late Jurassic-Early Cretaceous Maestrat Basin (Iberian Chain), *Geologica Acta* **14**, 2016a, 155-177.
- Nebot M. and Guimerà J., La extensión Triásica en el substrato de la Cuenca del Maestrat, y evidencias de tectónica salina en las evaporitas en facies Muschelkalk medio (Cadena Ibérica Oriental), *Geo-Temas* **16**, 2016b, 241-244.
- Ortí F. and Bayó A., Características litoestratigráficas del Triásico medio y superior en el “Baix Ebre” (Tarragona-España), *Cuadernos de Geología Ibérica* **4**, 1977, 223-238.
- Ortí F., García-Veigas J., Rosell L., Jurado M.J. and Utrilla R., Formaciones salinas de las cuencas triásicas en el Península Ibérica: caracterización petrológica y geoquímica, *Cuadernos de Geología Ibérica* **20**, 1996, 13-35.
- Ortí F., Pérez-López A., García-Veigas J., Rosell L., Cendón D.I. and Pérez-Valera F., Sulfate isotope compositions ($\delta^{34}\text{S}$, $\delta^{18}\text{O}$) and strontium isotopic ratios ($^{87}\text{Sr}/^{86}\text{Sr}$) of Triassic evaporites in the Betic Cordillera (SE Spain), *Revista de la Sociedad Geológica de España* **27** (1), 2014, 79-89.
- Ortí F., Pérez-López A. and Salvany J.M., Triassic evaporites of Iberia: sedimentologic and palaeogeographic implications for the western Neotethys evolution during the Middle Triassic-Earliest Jurassic, *Palaeogeography, Palaeoclimatology, Palaeoecology* **471**, 2017, 157-180.
- Salvany J.M., El Keuper dels Catalànids, petrologia i sedimentologia, (Graduate Thesis)1986, Universitat de Barcelona.
- Salvany J.M. and Ortí F., El Keuper de los Catalánides, *Cuadernos de Geología Ibérica* **11**, 1987, 215-236.
- Simms M.J. and Ruffel A.H., Synchronicity of *climate-climatic* change and extinctions in the Late Triassic, *Geology* **17**, 1989, 265-268.
- Solé de Porta N., Calvet F. and Torrentó L., Análisis palinológico del Triásico de los Catalánides (NE España), *Cuadernos de Geología Ibérica* **11**, 1987, 237-254.
- Song H., Tong J., Algeo T.J., Song H., Qiu H., Zhu Y., Tian L., Bates S., Lyons T.W., Luo G. and Kump L.R., Early Triassic sulfate drawdown, *Geochimica et Cosmochimica Acta* **128**, 2014, 95-113.
- Suárez Alba J., La Mancha Triassic and Lower Lias stratigraphy, a well log interpretation, *Journal of Iberian Geology* **33** (1), 2007, 55-78.
- Utrilla R., Pierre C., Ortí F. and Pueyo J.J., Oxygen and sulfur isotope compositions as indicators of the origin of Mesozoic and Cenozoic evaporites from Spain, *Chemical Geology* **102**, 1992, 229-244.
- Vecsei A. and Düringer P., Sequence stratigraphy of Middle Triassic carbonates and terrigenous deposits (Muschelkalk and Lower Keuper) in the SW Germanic Basin: maximum flooding versus maximum depth in intracratonic basins, *Sedimentary Geology* **160**, 2003, 81-105.
- Virgili C., El tramo rojo intermedio del Muschelkalk de los Catalánides, *Memorias y Comunicaciones Instituto Geológico Provincial de Barcelona* **13**, 1955, 37-78.
- Virgili C., El Triásico de los Catalánides, *Boletín. Instituto Geológico y Minero de España* **69**, 1958, 1-856.

Virgili C., Sopeña A., Ramos A. and Hernando S., Problemas de la cronoestratigrafía del Triás de España, *Cuadernos de Geología Ibérica* **4**, 1977, 57–88.

Wortmann U.G. and Paytan A., Rapid **V**ariability of **S** seawater **C**hemistry **O**ver the **P**ast 130 **M**illion **Y**ears, *Science* **337**, 2012, 334–336.

Queries and Answers

Query:

Please check the layout of Table 1 if correct.

Answer: Like in other tables, headings have been highlighted in bold character

Query:

Please check the layout of Table 3 if correct.

Answer: Yes

Query:

Please check the layout of Table 5 if correct.

Answer: Yes

Query:

Please check the layout of Table 6 if correct.

Answer: Yes

Query:

Your article is registered as a regular item and is being processed for inclusion in a regular issue of the journal. If this is NOT correct and your article belongs to a Special Issue/Collection please contact s.sankaran@elsevier.com immediately prior to returning your corrections.

Answer: Yes

Query:

Please confirm that given names and surnames have been identified correctly and are presented in the desired order, and please carefully verify the spelling of all authors’ names.

Answer: Yes

Query:

The author names have been tagged as given names and surnames (surnames are highlighted in teal color). Please confirm if they have been identified correctly.

Answer: Yes

Query:

Please check the hierarchy of the section headings and confirm if correct.

Answer: Yes

Query:

Citation "Castelltort, 1985" has not been found in the reference list. Please supply full details for this reference.

Answer: The correct citation is: Castelltort (in Marzo and Calvet, 1985). The change has been introduced.

Query:

Citation "Virgili (1985)" has not been found in the reference list. Please supply full details for this reference.

Answer: The correct citation is: Virgili (1958). This citation should appear in blue color.

Query:

The citation "Suárez, 2007" has been changed to "Suárez Alba, 2007" to match the author name/date in the reference list. Please check if the change is fine in this occurrence and modify the subsequent occurrences, if necessary.

Answer: The change is fine. The other occurrences have been also modified.

Query:

Uncited reference: This section comprises references that occur in the reference list but not in the body of the text. Please position each reference in the text or, alternatively, delete it. Thank you.

Answer: This reference appears in Fig. 15 but not in the text, We consider that this reference should be included in the references list.

Query:

Please check the page range in Ref. Korte et al., 2003.

Answer: The page range is correct.